12-1-1990

A CCD based bidirectional spectral reflectance field instrument

Michael H. Davis

A CCD BASED BIDIRECTIONAL SPECTRAL REFLECTANCE FIELD INSTRUMENT

by

Michael H. Davis
B. S. University of Maine
(1981)

A thesis submitted in partial fulfillment of the requirements for the degree of Master of Science in the Center for Imaging Science in the College of Graphic Arts and Photography of the Rochester Institute of Technology

December, 1990

Signature of the Author_____
Center for Imaging Science

Accepted by_____
Coordinator, M. S. Degree Program

Center for Imaging Science
Rochester Institute of Technology
Rochester, New York

CERTIFICATE OF APPROVAL

M. S. DEGREE THESIS

The M. S. Degree Thesis of Michael H. Davis has been
examined and approved by the thesis committee
as satisfactory for the thesis requirement for the
Master of Science degree

Dr. J.R. Schott, Thesis Advisor

Mr. J.F. Carson

Dr. Z. Ninkov

Mr. D.K. McCauley

Date 2/28/91

THESIS RELEASE PERMISSION FORM

ROCHESTER INSTITUTE OF TECHNOLOGY

COLLEGE OF GRAPHIC ARTS AND PHOTOGRAPHY

Title of Thesis

A CCD BASED

BIDIRECTIONAL SPECTRAL REFLECTANCE

FIELD INSTRUMENT

I, Michael H. Davis, hereby grant permission to the Wallace Memorial Library of the Rochester Institute of Technology to reproduce my thesis in whole or in part. Any reproduction will not be for commercial use or profit.

Signature:_____

Date: 3-1-91

A CCD BASED
BIDIRECTIONAL SPECTRAL REFLECTANCE
FIELD INSTRUMENT

by

Michael H. Davis

A thesis submitted in partial fulfillment of the requirements for
the degree of Master of Science in the Center for Imaging Science
in the College of Graphic Arts and Photography of
the Rochester Institute of Technology

ABSTRACT

Accurate interpretation and maximum use of multispectral data acquired from spaceborne and aircraft instruments require increased knowledge and understanding of the bidirectional reflectance distribution function (BRDF) of earth scene elements. Knowledge of the relationships between the spectral characteristics and important parameters of earth surface features can best be obtained by carefully controlled studies over areas, fields or plots where complete data describing the condition of targets is attainable and where frequent, timely spectral measurements can be made.

The Bidirectional Spectral Reflectometer (BuSTeR) described in this thesis was developed to provide the Digital Imaging and Remote Sensing Laboratory (DIRS) with the capability to obtain multispectral BRDF data from field targets. Topics in this thesis include the design goals of the optical, mechanical and electronic components, equipment calibration, options and capabilities provided through the software package and final performance evaluation of BuSTeR, including spectral resolution and responsivity, sensitivity to polarization, field of view, system linearity, noise performance and dynamic range.

ACKNOWLEDGEMENTS

The assistance of the following people was greatly appreciated and essential to the successful completion of this thesis:

Dr. John Schott, thesis advisor, for his material and moral support.

Mr. John Carson, thesis committee member, for his many hours of consultation.

Mr. Dave McCauley, thesis committee member, for his aid and advice with the analog and digital electronics.

Mr. Clair Luce, who provided significant mechanical design and construction support.

Mr. Klaus Fladt, who constructed both the differential to TTL interface board and the reference photodiode electronics package.

Messrs. Jeff Cotter and Drew Summers who graciously allowed me access to their computer equipment for code development and thesis documentation purposes.

Mr. Tim Gallagher, who provided mechanical and electrical construction support of the positioning system as well as valuable consultation.

Eastman Kodak Company, in particular Dr. J. R. Milch and Mr. W. J. Hutchinson, for providing me with the opportunity to earn the M.S. degree and for donating the front end electronics used for this device.

Table of Contents

Table of Contents (continued)

List of Figures

List of Tables

1. Introduction

Accurate interpretation and maximum use of multispectral data acquired from spaceborne and aircraft instruments require increased knowledge and understanding of the bidirectional reflectance distribution function (BRDF) of earth scene elements (Deering, 1986). It is desirable to provide field studies to determine the nature and magnitude of the natural surface reflectance variations relative to solar irradiance to subsequently improve our ability to interpret satellite data. Knowledge of the relationships between the spectral characteristics and important parameters of earth surface features can best be obtained by carefully controlled studies over areas, fields or plots where complete data describing the condition of targets is attainable and where frequent, timely spectral measurements can be made (Robinson, 1981). Measuring land surface parameters and their changes is a relatively simple task if the surface behaves as a Lambert plane, as the reflected radiance is then independent of the viewing direction (assuming a uniform area fills the field of view), and of the direction of the surface irradiation. Most vegetative ecosystems constitute complex surfaces that are non-Lambertian reflectors (Deering, 1988).

This thesis documents the Bidirectional Spectral Reflectometer (BuSTeR) which has been developed to provide the Digital Imaging and Remote Sensing Laboratory (DIRS) with the capability to obtain multispectral BRDF data from field targets. Topics in this thesis include the design goals of the optical, mechanical and electronic components, equipment calibration, options and capabilities provided through the software package and final performance evaluation of BuSTeR, including spectral resolution and responsivity, sensitivity to polarization, field of view, system linearity, noise performance and dynamic range.

Remote sensing of the earths surface consists of measuring the spectral radiance reflected from the surface, followed by the interpretation of the measured data in terms of physical features of the surface. The radiance received by the remote sensor is a function of the continuously varying incident

solar irradiance, atmospheric conditions and the reflectance properties of the surface (Jackson, 1987). A reflectance factor is defined formally as the ratio of the radiant flux actually reflected by a sample surface to that which would be reflected into the same sensor geometry by a lossless Lambertian surface irradiated in exactly the same way as the sample (Lillesand, 1987). The spectral bidirectional reflectance distribution function, $r(\theta,\theta',\phi)_\lambda$, is the three dimensional family of curves comprised of a series of reflectance factors at various angles, and is specified as a function of the relevant sun-object-camera angles (Schott, 1988) (figure 1-1). The spectral BRDF implies that the BRDF data is available as a function of wavelength.

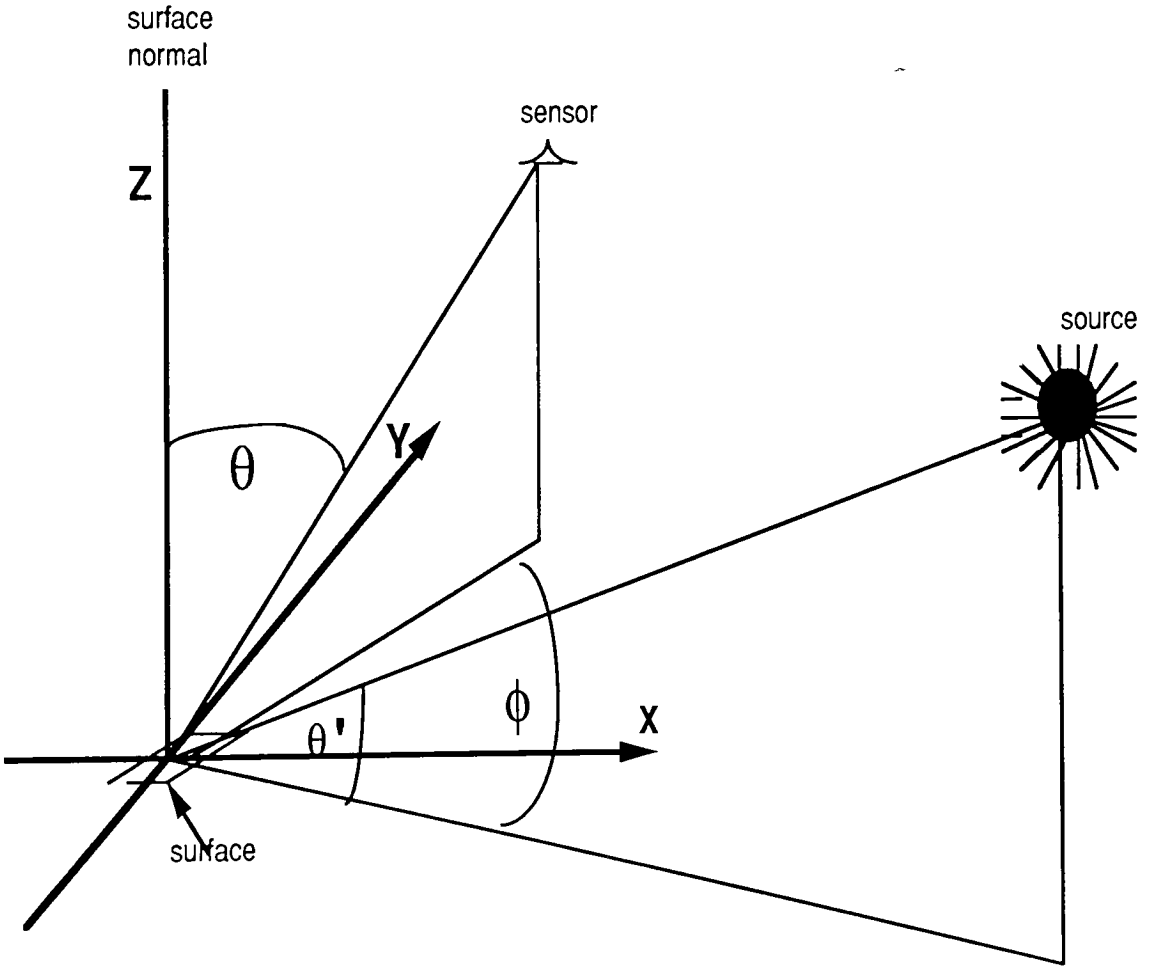

Figure 1-1 Source Object - Camera Angles

The bidirectional reflection distribution function can be expressed as:

$$r(\theta,\theta',\phi)_{\lambda}$$

where:

θ is the angle between the sensor and the normal to the surface.

θ' is the elevation of the source relative to the plane to the surface.

ϕ is the azimuthal angle between the source and the sensor projected into the plane of the object observed.

λ is the wavelength of illumination

In addition to direct solar reflection, the radiation scattered by the atmosphere diffusely irradiates the surface and is also reflected. This diffuse radiation can be very significant in the visible region of the electromagnetic spectrum, particularly in the blue portion of the spectrum.

1.1 Background

Many existing remote sensing satellites utilize spectral bands on the order of 0.1μm wide (see table 1-1), and the field BRDF reflectometers developed to date utilize the Landsat MSS spectral bands (Vanderbilt, 1987), TM spectral bands (Deering, 1986, Robinson, 1981, Deering, 1988) and a 1° or 15° field of view.

Donald Deering and Peter Leone (Deering & Leone, 1986) developed a field reflectometer, called PARABOLA, that utilizes two silicon and one germanium solid state detector along with bandpass filters to generate BRDFs corresponding to Thematic Mapper spectral bands 3, 4 and 5 (0.63 - 0.69, 0.76 - 0.90 and 1.55 1.75 μm). PARABOLA utilizes a 15° instantaneous field of view to sample a complete 4π sr hemisphere in 11 seconds. BuSTeR is sensitive over the 0.40 μm to 0.95 μm spectral range with 0.01 μm resolution, with a 1.5° field of view.

TABLE 1-1 Sensors, Sensitivity and Resolution

sensor type	mission	spectral bands (mm)	spatial resolution (m)
RBV	Landsat 1,2	0.475 - 0.575	80
		0.580 0.680	80
		0.590 0.830	80
	Landsat 3	0.505 - 0.750	30
MSS	Landsat 1-5	0.500 - 0.600	80
		0.600 0.700	80
		0.700 - 0.800	80
		0.800 1.100	80
	Landsat 3	10.40 - 12.60	240
TM	Landsat 4,5	0.450 - 0.520	30
		0.520 - 0.600	30
		0.630 - 0.690	30
		0.760 - 0.900	30
		1.550 - 1.750	30
		10.40 - 12.50	120
		2.080 - 2.350	30
HRV	SPOT 1	0.510 - 0.730	10
		0.500 - 0.590	20
		0.610 - 0.680	20
		0.790 - 0.890	20
AVHRR	NOAA 6-10	0.580 - 0.680	1100
		0.720 - 1.100	1100
		3.550 - 3.930	1100
		10.30 - 11.30	1100
		11.50 - 12.50	1100
CZCS	Seasat	0.430 - 0.450	825
		0.510 - 0.530	825
		0.540 - 0.560	825
		0.660 - 0.680	825
		0.700 - 0.800	825
		10.50 - 12.50	825

RBV Return Beam Vidicon camera
MSS Multi Spectral Scanner
TM Thematic Mapper
HRV High Resolution Visible
AVHRR Advance Very High Resolution Radiometer
CZCS Coastal Zone Color Scanner

Unlike PARABOLA, BuSTeR will never point up at the incoming radiation, so it has a separate photodiode to monitor changes in the solar illumination. A complete BRDF scan (~π / 3 sr) will take several minutes (5 - 30) depending upon the drive system.

B.F Robinson (Robinson, 1981) describes a Multiband Radiometer for Field Research which utilizes 8 spectral bands (0.45 - 0.52 μm, 0.52 - 0.60 μm, 0.63 - 0.69 μm, 0.76 - 0.90 μm, 1.15 - 1.30 μm, 1.55 - 1.75 μm, 2.08 - 2.35 μm, and 10.4 - - 12.5 μm), and the system can be set up for a 1° or a 15° field of view. Robinson's radiometer has a much greater spectral range than BuSTeR, but it has limited spectral resolution.

V.C. Vanderbilt (Vanderbilt, 1987), describes a field rated transmissometer used to rapidly determine the normal hemispherical transmittance of leaves at the four LANDSAT spectral bands. This device utilizes a commercially available Beckman DK-2A spectrophotometer with an integrating sphere attachment. This unit uses a commercially available radiometer, has a 2π sr field of view and uses a digital volt meter for data acquisition.

All of the above field BRDF reflectometers utilize silicon and / or germanium solid state detectors in conjunction with band-pass interference filters to obtain the desired spectral response. Todays hyperspectral remote sensors utilize the visible and infrared portions of the electromagnetic spectrum with spectral resolutions on the order of 10 nanometers and a range of 100 or more spectral bands (Goetz et al, 1985). Table 1-2 (Schott, 1989) lists today's hyperspectral imaging systems. This thesis presents BuSTeR, which is a spectral BRDF reflectometer designed for field use,sensitive from 400 nm to 950 nm capable of reporting spectral data with 5 nm,10 nm or 20 nm resolution. The reflected signal is obtained over a 1.5° field of view and is digitized to 14 bits, providing a wide radiometric dynamic range with high angular precision. The purpose of this reflectometer is to provide ground truth for the hyperspectral imaging systems.

Table 1-2 Hyperspectral Imaging Systems

system	sensor type	spectral range (μm)	spectral bandwidth (nm)	spatial resolution
AIS-2	2-D array	0.8 - 1.6 or 1.2 - 2.4	10	2.05 mrad / pxl
AVRIS	linear array	0.4 - 2.45	10	1 mrad / pxl
HRIS	push broom area array	0.4 - 2.5	10	30 m GIFOV
MODIS N	whisk broom scanner array	0.4 - 12	10	500 m or 1 km

Several quality radiometers are currently marketed (Photonics Buyers Guide) which, if fitted with the correct optics and mounted upon a positioning device, could easily be adapted to perform the function of a field BRDF reflectometer. For example, Geophysical Environmental Research Inc. manufactures the "Infrared Intelligent Spectroradiometer" which provides 350 nm to 3500 nm in a single scan with CPU controlled gain selection, or the Migdal Haemek "SR 5000 Intelligent IR Spectroradiometer" which can be used from 400 nm to 14500 nm and has auto-calibration and real time data analysis. These spectroradiometers are ideal candidates to use as spectral BRDF reflectometers, however they are quite expensive. BuSTeR utilizes a CCD imager and associated support electronics which were scrapped after an Eastman Kodak Research Labs project and an available monochrometer along with a purchased alt-azimuth telescope mount and PC-AT computer to provide a field instrument with performance parameters approaching the above mentioned laboratory instruments.

Table 2-1 lists the system performance specifications and some of the components used to achieve these specifications.

Table 2-1 Functional Specifications for BuSTeR

OPTICS	
CCD imager	Toshiba TCD 105C - 3648 8 μm x 8 μm active photosites on 8 μm centers with 4 adjacent photosites summed forming 912 8 μm x 32 μm pixel elements
Grating	400 lines per mm
Blaze Wavelength	550 nm
Reciprocal Dispersion	19.2 nm / mm
Total Spectral Range	550 nm (400 nm - 950 nm)
Spectral Resolution	5 nm, 10 nm or 20 nm
radiometric resolution	±0.001 reflectance units
Slit Width	0.28 mm for 5 nm resolution 0.6 mm for 10 nm and 20 nm resolution
Lens	20 mm focal length plano convex lens
Filters	Kodak Polycontrast PC-2 (balance filter) Kodak Wratten #24 (order sorting filter)
field of view (10 nm resolution mode)	1.7° x 0.06° (no slew) 1.7° x 1.6° (with slew)
MECHANICAL	
angular rotation declination rotation	 180° with a 0.00625° step resolution 180° with a 0.00625° step resolution
Angular Velocity	1.5 degrees per second

A block diagram of the system components is shown in figure 2-1. The 'camera head' consists of an Oriel 7240 grating monochrometer with a 400 line per millimeter grating blazed at 550 nm. The monochrometer is modified to accept a Toshiba TCD 105C CCD imager which consists of 3648 8 μm by 8 μm active photosites on 8 μm centers. Four adjacent photosites are summed per pixel, resulting in **912 8 μm by 32 μm pixel elements**. The grating efficiency, CCD response and balance filter transmission characteristics combine to provide a **spectral range** of **400 nm to 950 nm**, while the grating groove spacing and input slit width have been chosen to provide **10 nm resolution.**

When all 912 pixels are used, the system is capable of digitally sampling to 0.6 nm resolution. Since a 0.5 mm slit limits the systems response to 10 nm, we can sum together 16 pixels and not change the spectral resolution of the system. If a higher resolution is desired, one simply inserts a smaller slit and sums less pixels (eg. 5 nm resolution can be achieved by using a 0.25 mm slit and summing 8 pixels).

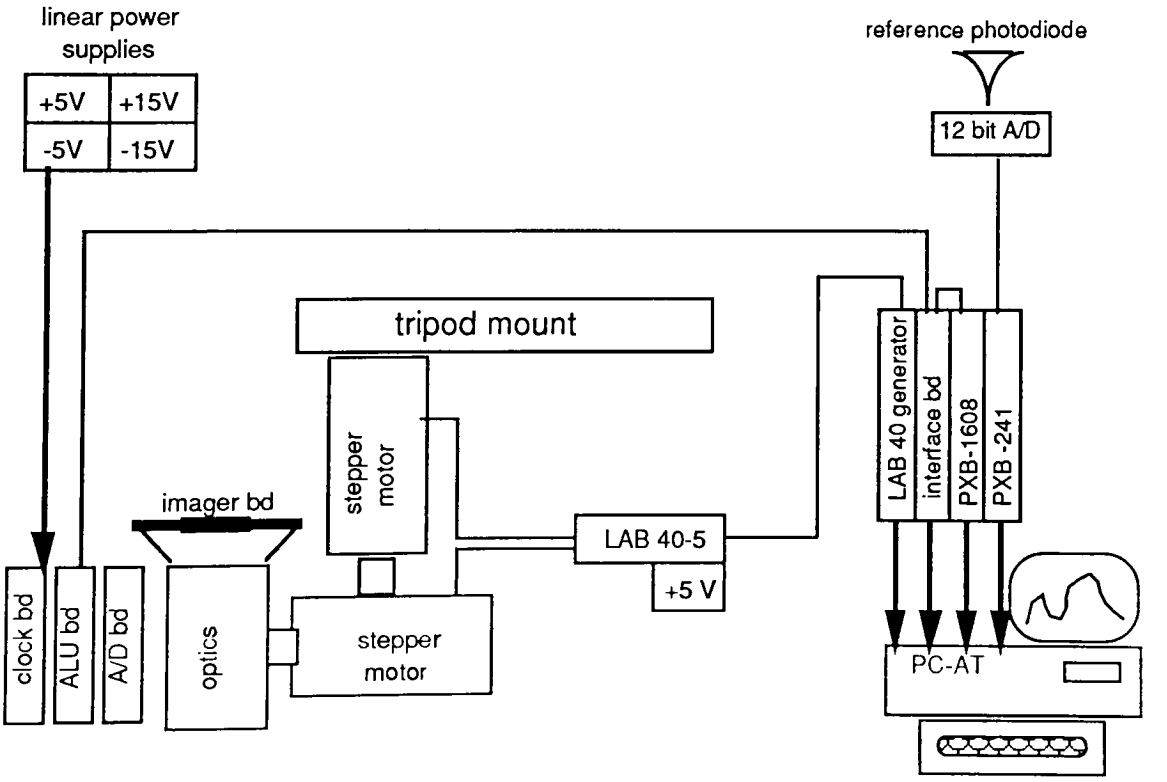

Figure 2-1 System Block Diagram

The reflection efficiency of the diffraction grating is polarization dependent, therefore the BRDF of a sample that polarizes light upon reflection will not be accurately represented. In order to compensate for this shortcoming, a fiberoptic faceplate is used to randomize any polarization preference.

The electronics utilizes a dynamic switching scheme which employs either analog or digital summing of four photosites, based upon signal level, to increase the dynamic range of the system. Signals over 1/8 full well are individually digitized and then digitally summed on the arithmetic logic unit (ALU) board, while signal levels under 1/8 full well are summed in the analog domain at the output stage of the CCD imager. All signals are digitized via a Burr-Brown ADC600 12 bit analog to digital (A/D) converter, resulting in a **14 bit digital output** per pixel after summation.

The camera head, A/D converter and ALU board are attached to an alt-azimuth telescope mount and suspended approximately 4 feet above the target by means of a tripod. Two stepper motors control the two axis positioning system which can aim the camera in any desired direction. As the various angles are sampled, the reflectometer will view different locations on the target, so the target must have a radius of at least 4 $\tan(\theta)$ feet, where θ represents the largest sample declination angle measured from the normal. The field of view of the system is a function of the input slit width (0.5 mm) in the direction parallel to the CCD array and a function of the CCD imager photosite width (0.008 mm) perpendicular to the CCD array, resulting in a rectangular field of view. A square field of view is desired, so the system utilizes a cylindrical lens mounted in front of the the CCD imager to provide an anamorphic image in the plane of the CCD imager.

The optical path (figure 2-2) begins with a 20 mm focal length plano-convex objective lens which focuses light reflected from the target onto a fused fiber optic faceplate (figure 2-3). The diffraction grating efficiency is dependent

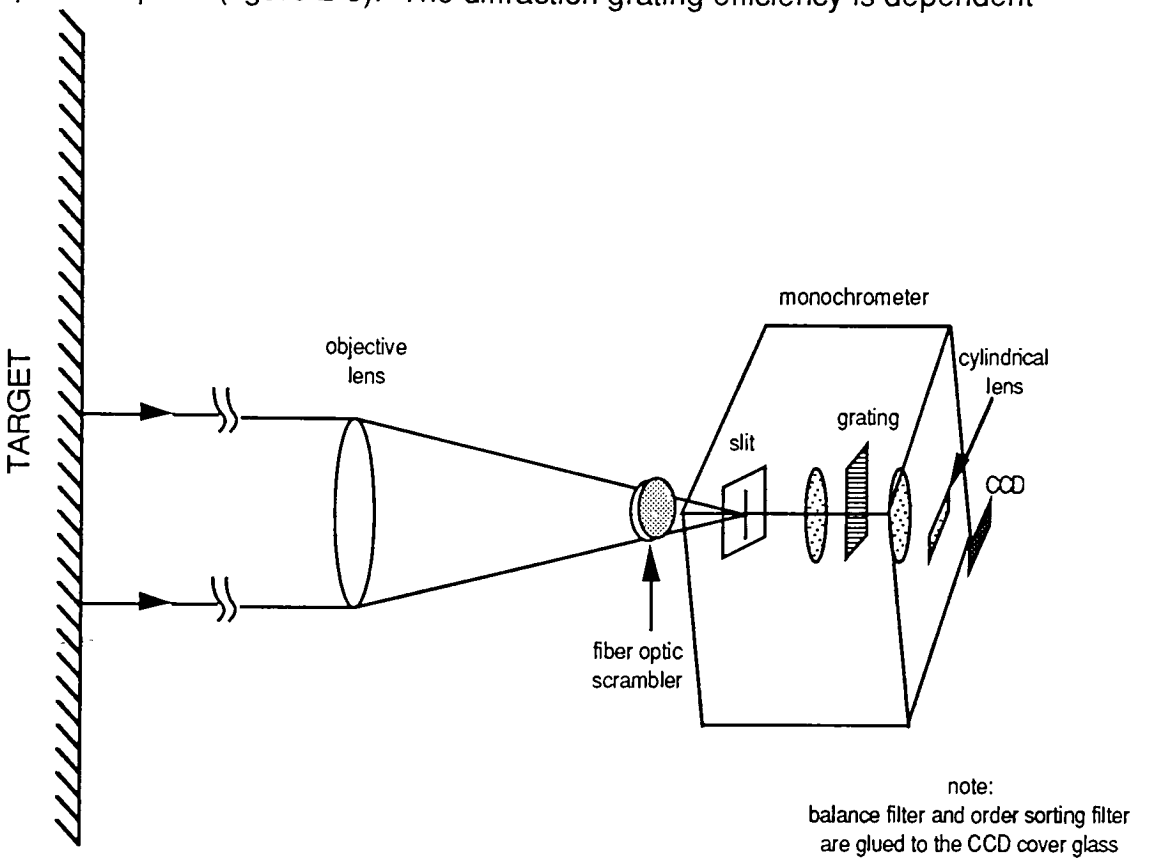

Figure 2-2 Optical Path

upon the polarization angle of the incident light , and the coherent fiber-optic faceplate (figure 2-3), which is 0.25" long and made up of 0.002" diameter fibers (N.A. = 0.66), is used to randomly polarize (or scramble) the light reflected from the target (see section 5, Test Results and Analysis, for scrambler efficiency).

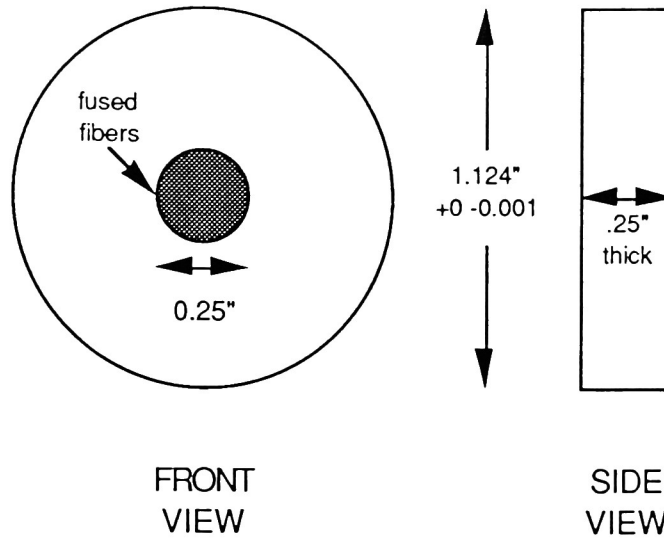

Figure 2-3 Fiber Optic Scrambler

After passing through the fiber optic scrambler, the light is presented to the Oriel 7240 monochrometer which passes the incoming radiation through the entrance slit, collimates the radiation and directs it to a diffraction grating (figure 2-4). The diffracted spectrum is focused onto the plane of CCD imager (which replaces the exit slit of the monochromator) so each end of the desired spectrum is aligned with each end of the CCD imager. The grating is ruled with 400 lines per mm, which results in a center to center spacing (a) of 2.5 microns. The reciprocal dispersion of this setup is 19.2 nanometers per millimeter and the optical elements on either side of the grating have the same focal length resulting in a magnification factor of unity.

The actual monochromator optics uses spherical mirrors to create the folded optical path shown in figure 2-5. The optical paths shown in figures 2-2 and 2-4 are refraction models of the mirror optics, and are used to illustrate points which are independent of the physical optical elements.

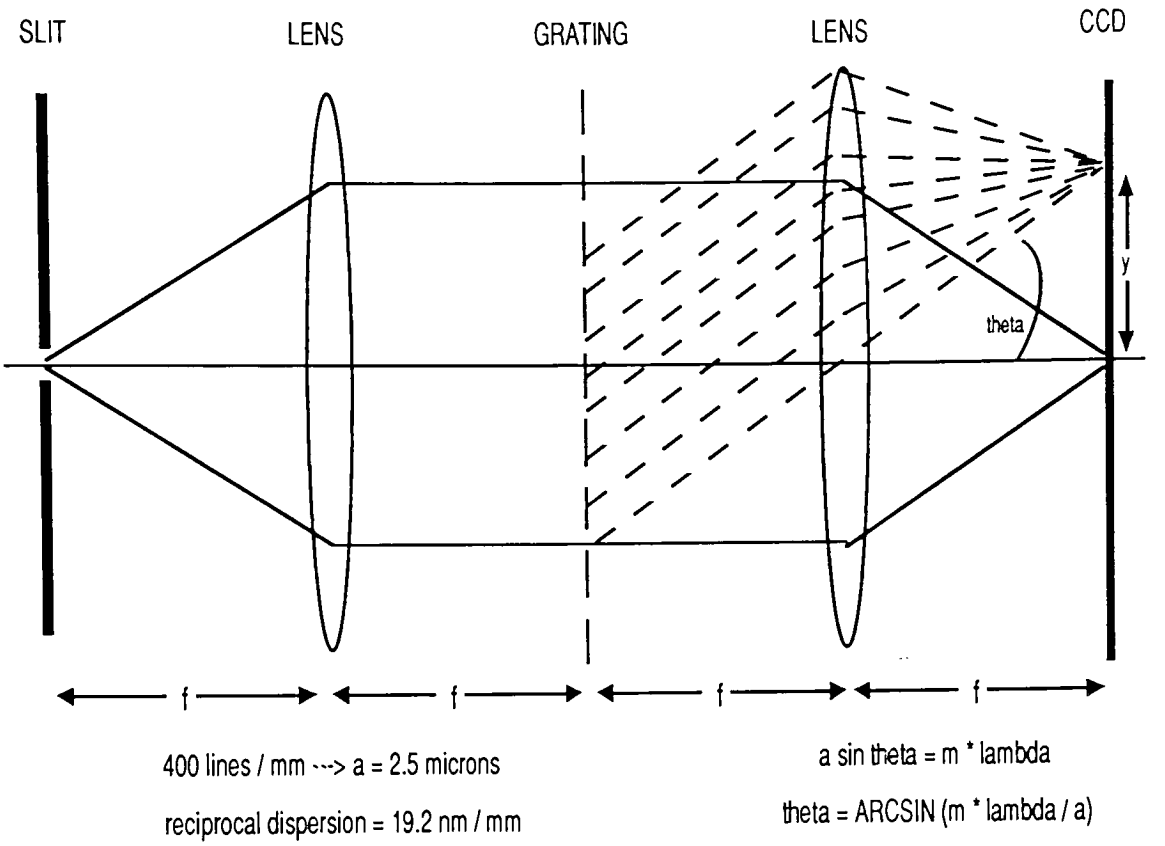

Figure 2-4 Dispersion Optics

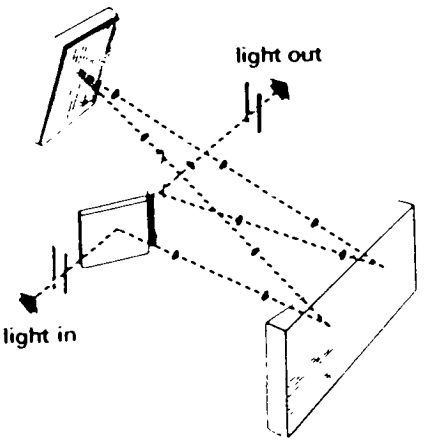

Figure 2-5 Actual Monochromator Optical Path

Figure 2-6 shows that the 400 nm signal from the second order diffraction overlaps the 800 nm signal from the first order, requiring an order sorting filter. A Kodak Wratten #24 filter blocks light below 580 nm, and this filter is glued over all photosites measuring radiation of 700 nm and above.

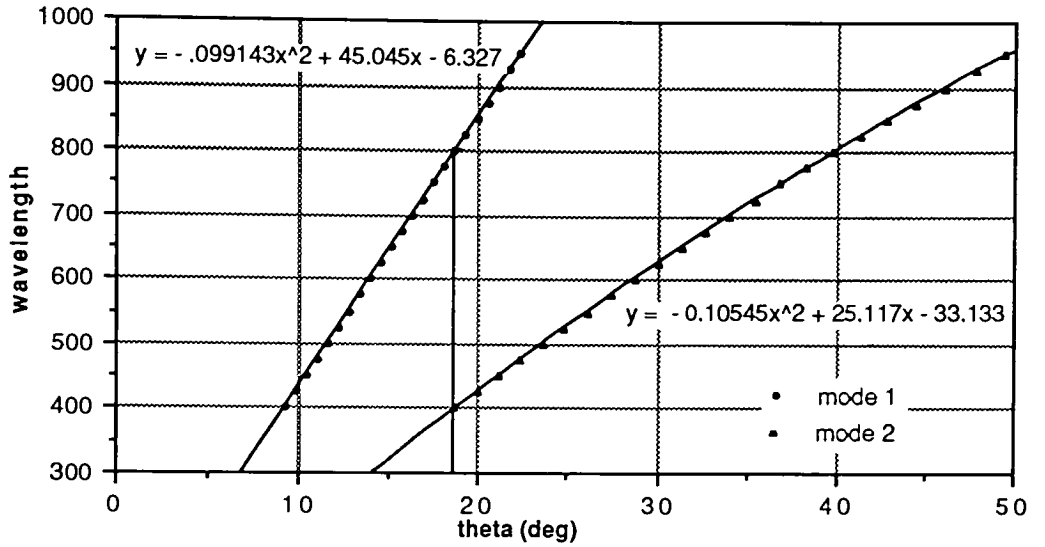

Figure 2-6 Angular Dispersion

Figure 2-7 shows the efficiency of the diffraction grating, CCD response and PC-3 balance filter characteristics, while figure 2-8 shows the total system response after combining these three components.

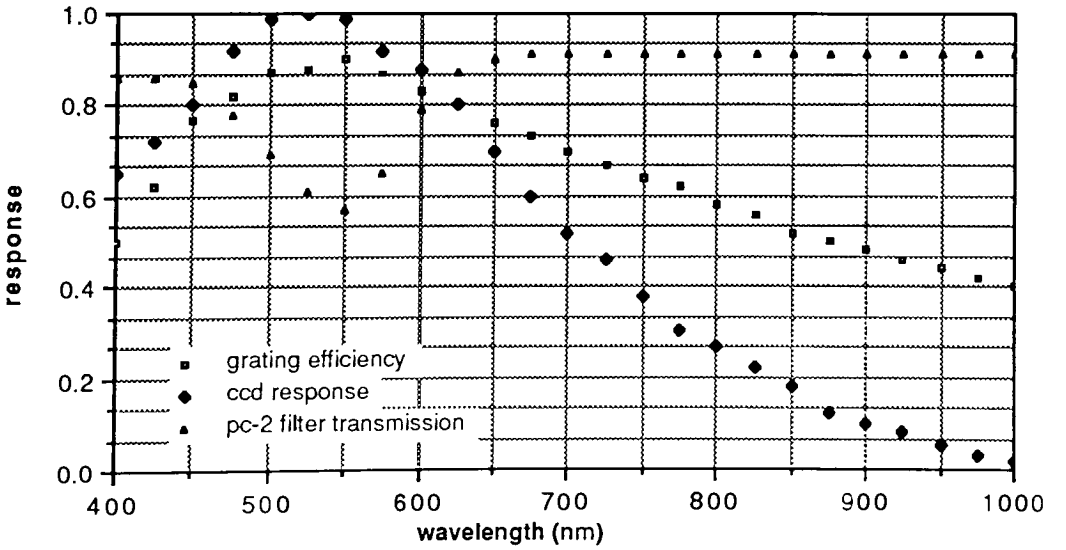

Figure 2-7 Spectral Response of System Components

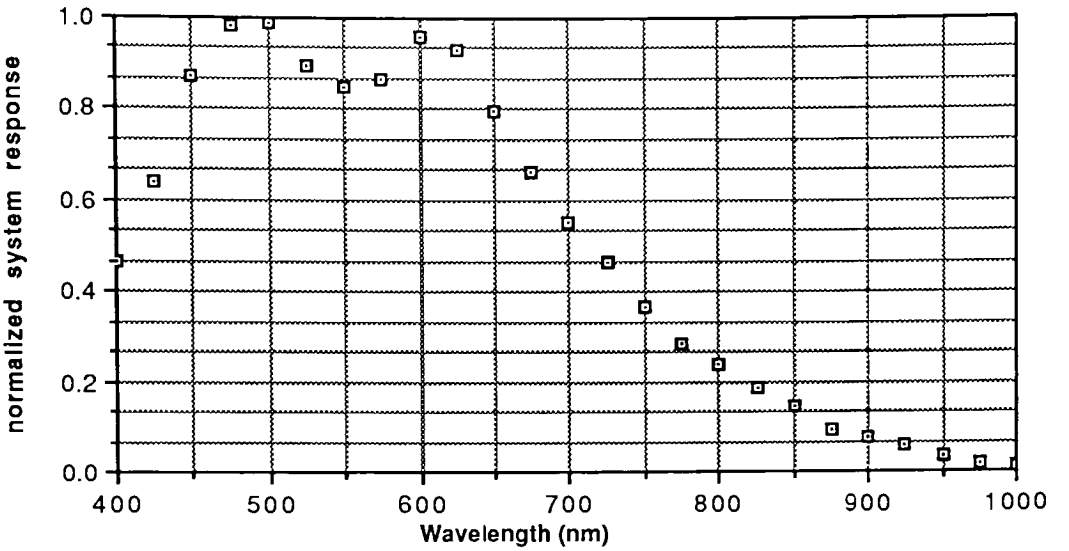

Figure 2-8 System Spectral Response (normalized)

Our goal is to measure BRDFs over a 400 nm to 950 nm spectral range, and the response peak at 550 nm will inhibit our ability to 'see' out to 950 nm, so the PC-2 balance filter is glued over the photosites which are sensitive over a 400 nm to 700 nm spectral range (it is butted up against the order sorting filter). The order sorting filter is not explicitly shown in these graphs since the net effect of this filter on wavavelenghts above 700 nm is the same as the balance filter.

The 912 CCD pixel elements encompass the spectral range of 400 nm to 950 nm enabling a maximum theoretical resolution of 0.6 nm, hence, the user can change the resolution of the system by simply changing the input slit width. We currently have two slit sizes available, 0.28 mm and 0.6 mm, providing system resolutions of 5.6 nm and 11.2 nm respectively. The bulk of the work done for this thesis utilizes the 0.6 mm slit, allowing a maximum resolution of 11.2 nm, however the data is reported at 10 nm increments. Since each photosite resolves 0.6 nm, 16 photosites are summed to provide the 10 nm resolution (see section 2.2).

Figure 2-9 is a sketch (Smith 1966) of a simple radiometer. The detector, with diameter d, is located at the focus of an objective with focal length F and diameter A.

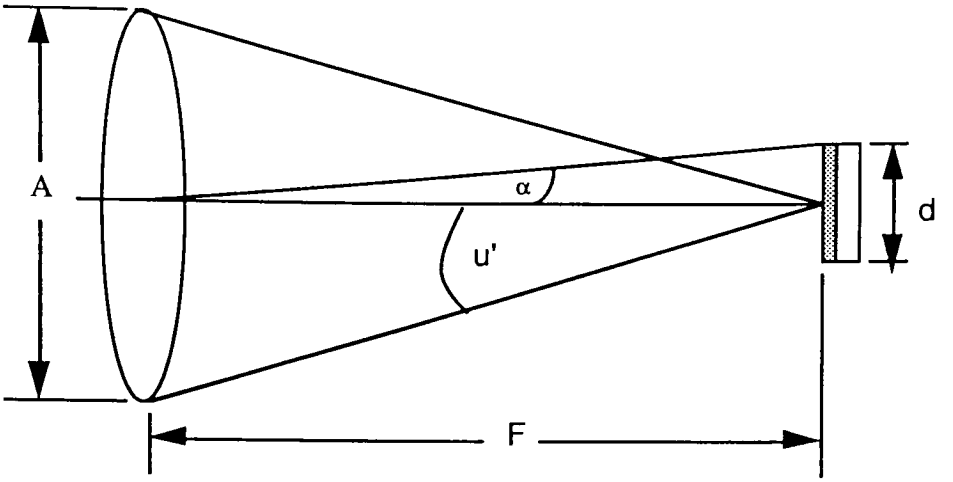

Figure 2-9 Field of View Geometry

The half-field of view of the system is α, and since the detector is at the focus of the system, that half-field of view is given by

$$\alpha = d / 2F$$

The monochromator limits the throughput of the system to f / 3.7, resulting in an effective aperture (limited by the monochromator) of

$$A = F / f/\# = 20 \text{ mm} / 3.7 = 5.4 \text{ mm}$$

The effective f/# of the objective (limited by the detector) is

$$(f/\#) = F / A = d / (2 A \alpha)$$

solving the above equation for the half-field if view (α) yields

$$\alpha = d / (2 A f/\#)$$

since, in this system, the f/# = 3.7 and A = 5.4 mm, inserting d in mm we get

$$f.o.v = 2\alpha = d / 19.98 \text{ (radians) or } 2.868 * d \text{ (degrees)}$$

The optical head on BuSTeR can be modeled in the direction parallel to the CCD elements by setting the detector diameter d equal to the input slit width. When using the 0.6 mm slit, the field of view is 1.72 degrees. The field of view in the direction perpendicular to the CCD array is limited by the width of the photosites, 0.008 mm, yielding a field of view of 0.023 degrees. Since this field of view is limited by the size of the photosites, and not the collection optics, we can increase the field of view in this direction (and increase our signal) by changing the size of the photosite in this direction. There are CCD arrays available with rectangular photosites, but budgetary considerations limit us to the Toshiba CCD imager. The input slit for the monochromator is 5 mm long, resulting a 5 mm wide spectrum at the CCD. The approach taken here is to modify the aspect ratio of the field of view by condensing some of the energy passed through the 5 mm long input slit with a cylindrical lens, optically elongating the detector height.

The cylindrical lens is a polished quartz rod with a radius r = 4.95 mm and index of refraction n = 1.44. The thick lens formula for a spherical lens can, for this situation ($r_1 = r_2 = r$) , be represented by:

$$\begin{aligned} 1/f &= (n - 1) [1/r + 1/r - 2r(n-1) / (nr^2)] \\ &= 2(n - 1)/r [1 \quad (n - 1) / n] \\ &= 2(n-1) / (nr) \end{aligned}$$

or

$$f = nr / [2(n-1)]$$

for our quartz rod, n = 1.44 and r = 4.95 mm so:

$$f = 8.1 \text{ mm}$$

The quartz rod is positioned in the system (figure 2-10) such that it magnifies the photosites (condenses the output spectrum) in the direction perpendicular to the spectral distribution by a factor of 2.5 resulting in an effective detector height of 0.2 and a final field of view of 1.72° x 0.06°. Once again, figure 2-10 uses refractive lenses in place of the actual reflection optics for illustrative purposes.

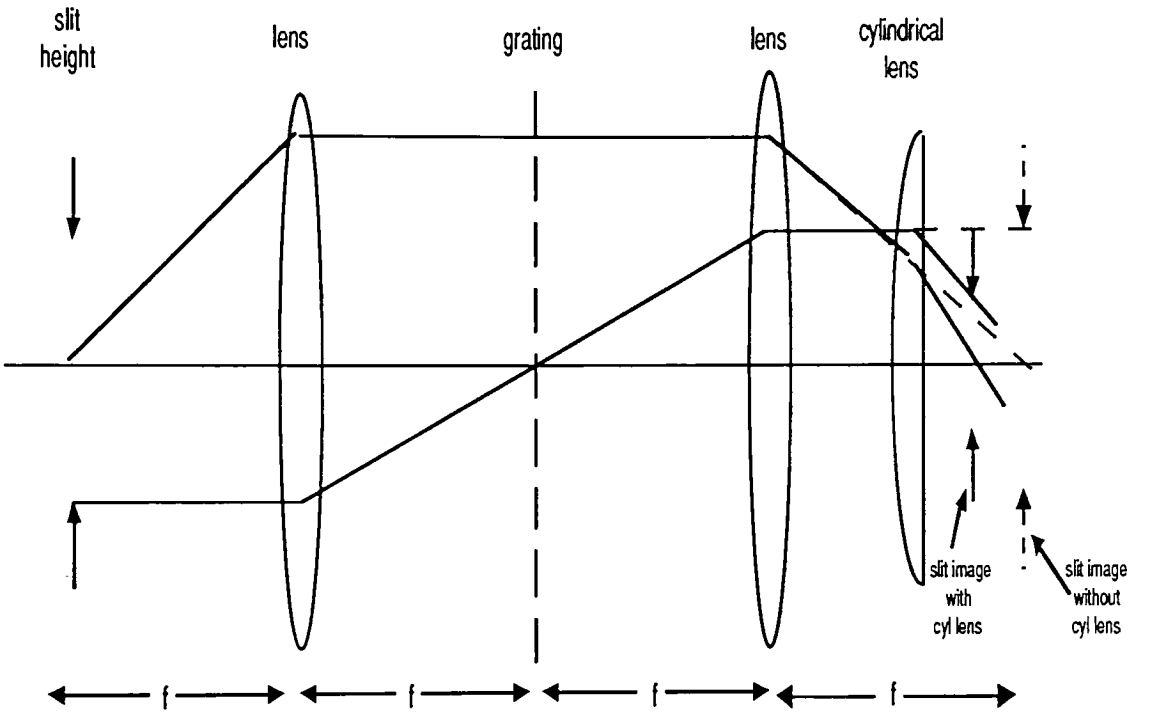

Figure 2-10 Cylindrical Lens in Monochromator

There is also a software option called "slew scan" which sums 8 scans, each scan repositioned 0.2 degrees in the narrow field of view direction, providing a 1.72° x 1.6° field of view.

The spectral resolution for BuSTeR can be derived using the spatial features of the system and the reciprocal dispersion (19.2 nm / mm) of the monochromator optics. The input slit width and output sampling aperture can each be varied to provide the user with a range of spectral resolution options. The limit of spectral resolution is the smallest interval $\delta\lambda$ between two just distinguishable wavelengths, and the Rayleigh criterion, which was established for the theoretical case of pure Fraunhofer diffraction, defines $\delta\lambda$ as the difference between the maximum and the first zero of the diffraction pattern (Girard). A simple criterion used in practice defines the spectral resolution limit $\delta\lambda$ to be the full width at half maximum (FWHM figure 2-11).

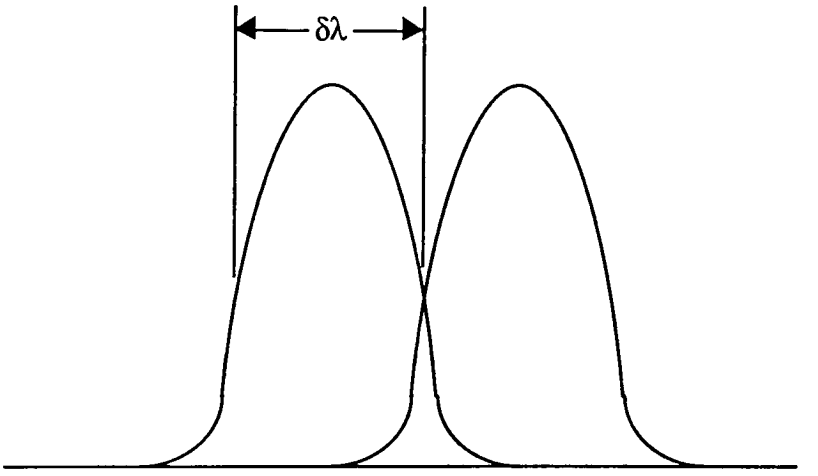

Figure 2-11 Full Width Half Maximum (FWHM) Resolution

A schematic diagram for the dispersing system is depicted in figure 2-4. The light distribution in the final focal plane f(y) is a convolution of the dispersion of the system d(y) with the input slit function $s_1(y)$, which is a rectangular function

$$f(y) = d(y) * s_1(y)$$

of unity height and width equal to the input slit width (a). Furthermore, the digitized spectral response of the system is the convolution of the light

distribution in the final focal plane with the sampling aperture function $s_2(y)$ which is also a rectangular function of unity height and width equal to the sampling aperture width (w). The final spectral response of the system g(y) is:

$$g(y) = s_2(y) * f(y) = s_2(y) * d(y) * s_1(y)$$

Since the convolution operation is both commutative and associative, the impulse response of this system (replace d(y) with a delta function) is:

$$g(y) = s_1(y) * s_2(y) * \delta(y) = s_1(y) * s_2(y)$$

The minimum sampling aperture for BuSTeR is .032 mm, and since the reciprocal dispersion is 19.2 nm per mm, this equates to a spectral bandpass of 0.6144 nm. Using the input slit width of 0.6 mm (bandpass = 11.52 nm) we see that the input slit width for the system is 18.75 times the minimum sampling width. Figure 2-12 shows that the impulse response of a system using a sampling aperture which is much smaller than the input slit width

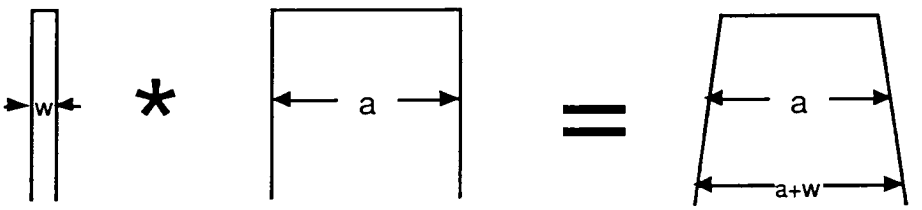

Figure 2-12 Impulse Response when Sampling Aperture << Slit Width

while figure 2-13 shows the impulse response of a system using a sampling aperture which is equal to the input slit width.

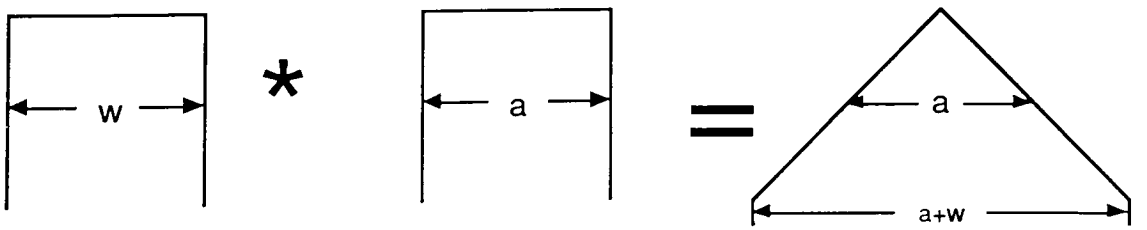

Figure 2-13 Impulse Response when Sampling Aperture = Slit Width

Application of the FWHM resolution criteria to each of these cases shows that the resolution for this system is always equal to the input slit width provided the sampling aperture is less than or equal to the input slit width. In the 10 nm resolution mode BuSTeR uses a sampling aperture of 0.512 mm (sum 16 photosites) with the 0.6 mm slit (actual FWHM resolution is 11.52 nm) and in the 5 nm resolution mode a 0.28 mm slit is inserted and 8 photosites are summed (0.256 mm sampling aperture) providing an actual FWHM resolution of 5.38 nm.

2.3 Electronics

The Toshiba TCD105C CCD image sensor has an output saturation voltage of 0.8 V and a DC offset of +5 V. The analog electronics on the imager board is used to offset and amplify this signal so that it fits into the -1.25 V to +1.25 V range of the A/D converter. The DC offset adjustment potentiometer is denoted as R-27 and is physically located beside the Comlinear CLC-200 op-amp closest to the analog output connector (J-6). The gain adjustment potentiometer is denoted as R-17 and is located slightly behind the CLC-200. There is an unused potentiometer on this board, R-21, which is located closest to the middle of the board. Figure 2-14 shows the layout of the CCD imager board including

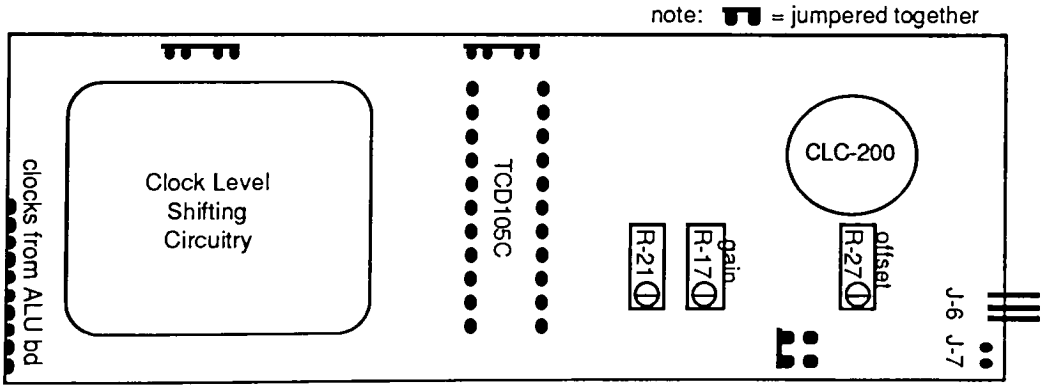

Figure 2-14 CCD Imager Board Layout

potentiometer placements, jumper configurations and connector locations. Connector J-7 is an output signal test point with the signal on the inside pin and the ground located closest to the edge of the board.

The output from the CCD imager board is sent to a 12 bit Burr-Brown ADC600 A/D converter and the digitized signal is then sent to the arithmetic logic unit (ALU) board which performs digital correlated double sampling and summing for four photosites (see Appendix A). The ALU board has 18 outputs which are all differential TTL and consist of a 14 bit data word with a sign bit, a mode bit (analog or digital summing), a data valid pulse and a new line pulse. These signals are interfaced to the Hewlett Packard Vectra ES/12, which is a 12 MHz, hardware compatible IBM PC clone. The data from the ALU board is first sent to the differential to TTL conversion board, which is a custom board designed for this application, and the each of the 18 differential pair signals is converted to a single TTL level digital signal. This differential to TTL conversion board is wirewrapped onto a PC compatible board and resides in the left most slot of the HP Vectra backplane. The TTL data is then sent to a Qua Tech PXB-1608, which is a true 16 bit digital I/O board with direct memory access (DMA) capabilities. The new line pulse is used to synchronize the DMA cycle and the data valid pulse is used to latch each 14 bit data word with the associated sign and mode bit and trigger the DMA cycle. Complete schematics and/or user manuals for each of these boards is in the documentation package.

An EG&G UV250BG photodiode is used as the reference device which tracks solar illumination variations. This photodiode is operated in photoconductive mode for optimum linearity and frequency response. The output current from the photodiode is sent to an OP-07 operational amplifier which converts this current to a voltage level and this voltage is then presented to an Analog Devices AD574A complete 12 bit successive-approximation analog-to-digital converter. The A/D converter is interfaced to a Qua Tech PXB-241 digital I/O board, using port C pin PC4 for the output strobe to start the A/D converter, and port A pins PA7 - PA0 for the 8 most significant input bits (11 - 4) and port B pins PB3 - PB0 for the 4 least significant bits (3 0). The photodiode and associated electronics receives power from the same linear power supplies used fro the front end electronics.

The relationship between declination angle, inclination angle and azimuth (rotation angle) are shown in figure 2-15. All BRDF azimuth readings will correspond to 0 = true north, and all declination readings will correspond to 0 = straight down (nadir).

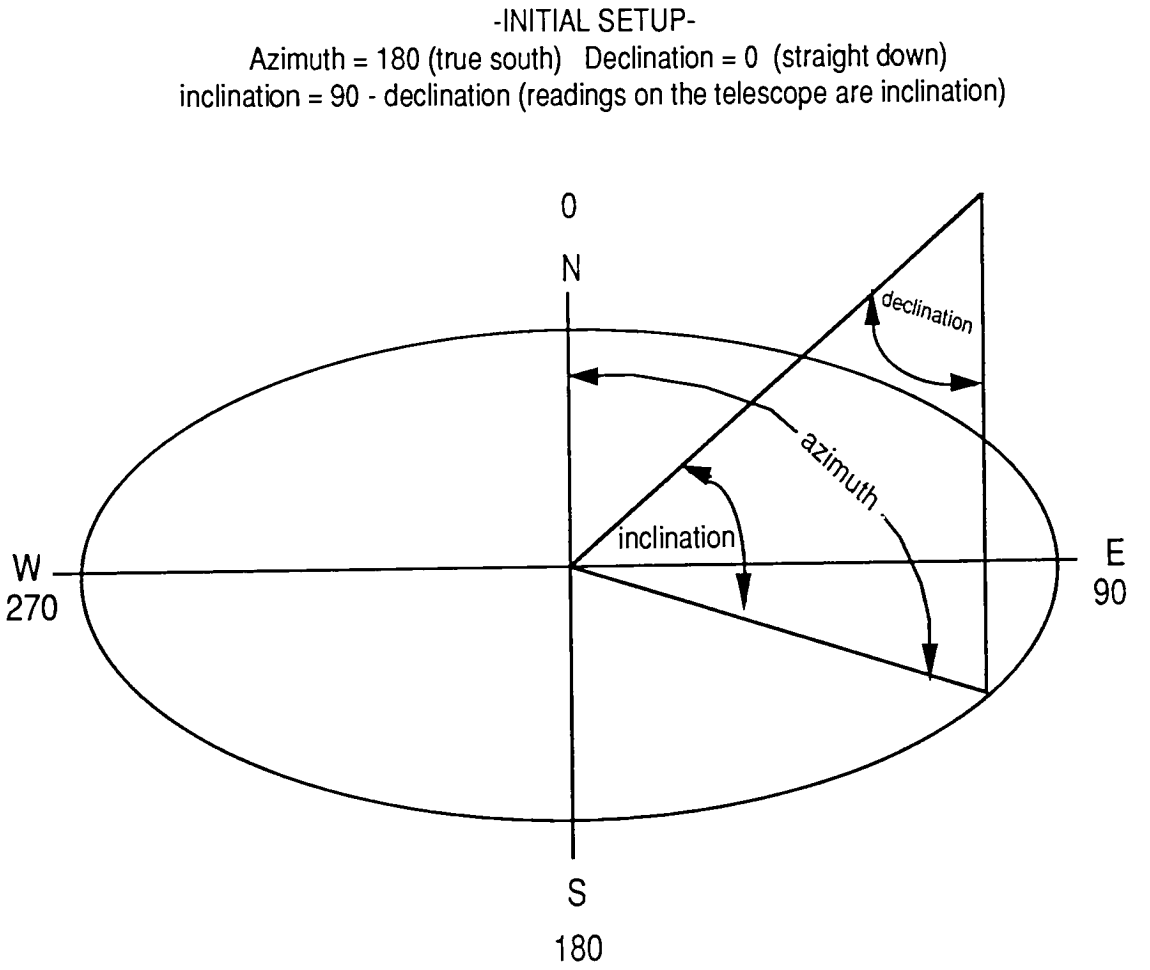

Figure 2-15 Declination and Azimuth Angles

The camera head, A/D converter and ALU board are all attached to an equatorial (alt azimuth) telescope mount and suspended approximately 4 feet

above the target by means of a tripod (figure 2-16). The two stepper motors control the declination (alt) and rotational (azimuth) axes of the positioning system, aiming the camera in any desired direction.

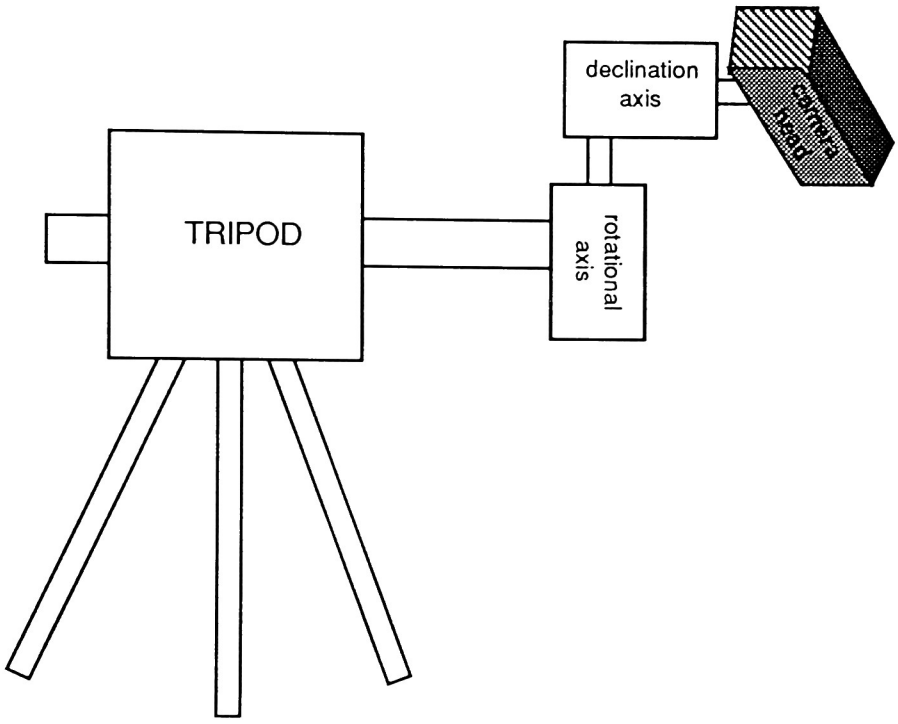

Figure 2-16 BuSTeR Positioning System

A full BRDF consists of rotational data over 360 degrees for each inclination angle. The tripod blocks us from rotating a full 360 degrees, so 180 degree rotational data is acquired for plus *and* minus declination angles, giving us full BRDF scans (figure 2-17). The bold typed angles in figure 2-17 are acquired using positive declination angles and direct azimuth readings, while the other angles (outside the 80 to 260 degree azimuth range) are acquired using negative declination readings and the BRDF azimuth angle is 180 degrees opposite the systems actual rotational angle. As the various angles are sampled, the reflectometer will view different locations on the target, so the target must have a radius of at least 4 $\tan(\theta)$ feet, where θ represents the largest sample angle measured from the normal.

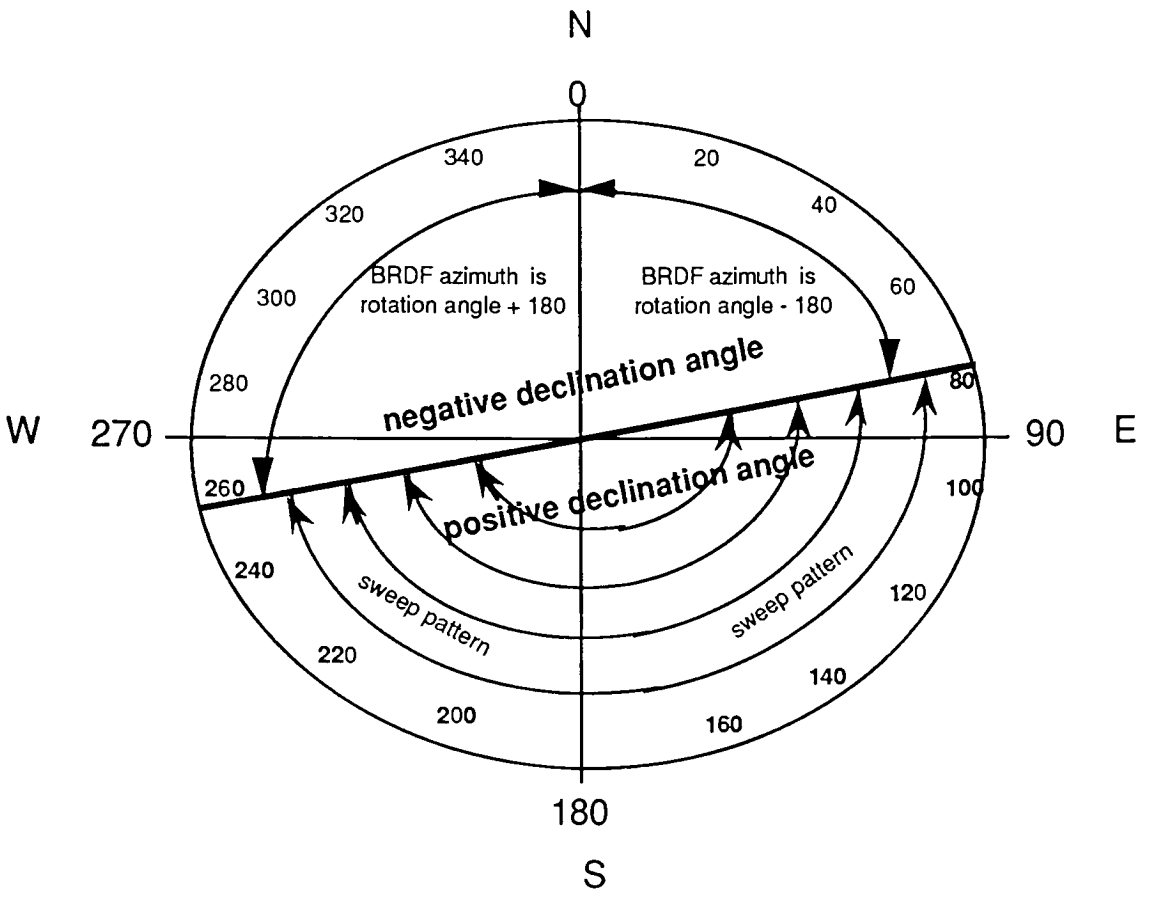

Figure 2-17 Rotational Position and Azimuth

During BRDF acquisition cycles, BuSTeR will always start with a positive declination angle and rotate from 80° to 260° minus the angular increment, taking data at the specified angular increments. Upon reaching 260° minus angular increment, BuSTeR will position the declination axis to the negative declination angle and rotate from 260° minus angular increment back to 80°, again taking data readings at the desired angular increments. The readings acquired on the return trip will be mapped to correct BRDF readings. Figure 2-18 presents an example for mapping rotational readings and declination readings to the associated BRDF azimuth angles when the angular increment is 20°. The 80° and 260° endpoints are used since they are evenly divisible by the available 5° , 10° and 20° angular increments.

NOTES:

BRDF always starts at 80, and rotates to (260 - anglular increment)
with positive declination angle (declination reading > 90).

Next, the declination angle is reversed (90 - declination on the telescope mount)
and the rotation angle is moved from (260 - angular increment)
to 80 corresponding to BRDF azimuth readings
(80 - angular increment) to (260 + angular Increment).

EXAMPLE: angular increment = 20

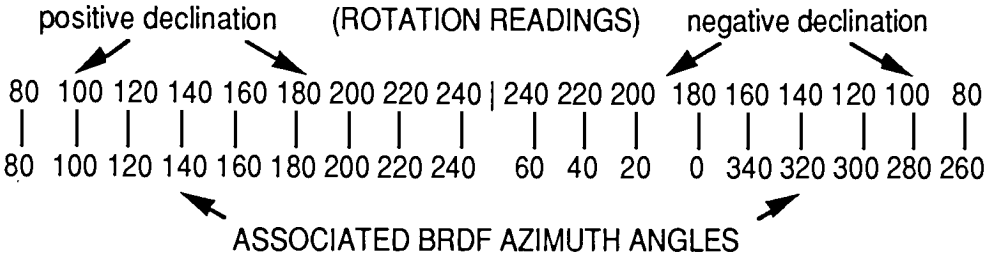

The BRDF azimuth angles are not generated in chronological order, so the program has to load the BRDF buffer in a somewhat complicated manor.

Figure 2-18 Relationship Between Rotation Angle and BRDF Azimuth

As mentioned earlier, a reflectance factor is defined formally as the ratio of the radiant flux actually reflected by a sample surface to that which would be reflected into the same sensor geometry by a lossless Lambertian surface irradiated in exactly the same way as the sample. In order to achieve this ratio, dark and gain calibrations must be computed and applied to remove constant system abnormalities.

Dark calibration is necessary to define the zero point (or y offset) of the response function for each pixel. The necessary data is acquired by using a shutter to eliminate the incoming radiation, and each individual pixel reading is stored in a file. This dark value is subtracted from each and every pixel reading, including readings taken to generate the gain data.

Gain calibration is necessary to determine the slope of the response function for each pixel. In this system, changing wavelength is analogous to changing pixels, so functions that vary with wavelength, vary across the CCD. The computed gain value is ultimately used to correct for pixel to pixel variations in the CCD due to the photodiode's spectral response, the efficiency of the diffraction grating and source illumination nonuniformity. The raw gain data is obtained by reading a calibrated reflectance panel, which is **a** 6" by 6" white Spectralon reflector supplied by DIRS, at camera declination angle $\theta = 0$ degrees (nadir) and solar incident angle derived from the solar altitude θ' and solar azimuth ϕ. The gain factor is computed for each pixel such that, when multiplied times the actual reading, results in the calibrated BRDF reading for the target (for the current θ, θ' and ϕ) times 1000. The calibration reading need only be acquired at one set of θ, θ' and ϕ, and the computed gain for each pixel (wavelength) of the system resulting from this reading will be applied on a pixel by pixel basis. This reading, and all subsequent readings, will be accompanied by a reading from the reference photodiode (minus it's dark reading) to determine relative variations in source intensity.

The reference reading must be factored into the original gain readings to compute the gain corrections multiplication factor, which is given by:

$$PGF = 1000 * [r'(\theta,\theta',\phi)_\lambda \ / \ (I' - D)]$$

PGF	= pixel gain factor
$I'(\theta,\theta',\phi)_\lambda$	= raw gain reading from the reflectance panel
$r'(\theta,\theta',\phi)_\lambda$	= panel reflectance (actual floating point fractional value)
D	= dark corrections value
g	= current photodiode reference reading (minus dark)
g'	= original photodiode reference reading (minus dark)
n	= number of bits to define full well signal (14 in our case)

Each and every pixel, the final spectral BRDF reading is given by:

$$r(\theta,\theta',\phi)_\lambda = (reading - D) * PGF * (g' / g)$$

Which is the actual BRDF times 1000 (the output data file has integer values).

The nadir reflectance of the Spectralon calibration panel has been experimentally determined by (Feng 1990) to be:

$$1.1148 \quad .0046232\,\alpha + 0.000083317\,\alpha^2 - 0.000000899665\,\alpha^3$$

where α is the incident angle of the light hitting the Spectralon measured from the normal to the surface.

The optics for BuSTeR is setup to measure spectral radiance, L_λ, which is the flux per unit projected area per unit per unit solid angle per spectral band

leaving a surface. $d^2\Phi$ is the flux emitted into a solid angle $d\Omega$ by a surface element of projected area dA_{proj} (figure 3-1)

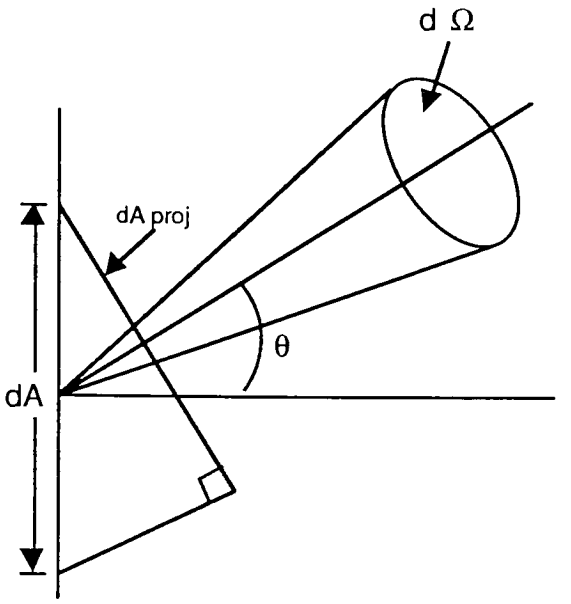

Figure 3-1 Projected Area in Radiance Definition

$$dA_{proj} = dA \cos \theta$$

where θ is the declination angle (from nadir). The radiance theorem states that radiance is conserved for propagation through a lossless optical system, and can be proved (Boyd 1987) for the special case of propagation through a homogeneous medium. Our final spectral BRDF reading is the result of taking the ratio of the current target reading with the gain corrections reading hence the transmission characteristics of the optical path are nulled out (for unpolarized reflections).

A lambertian source is an incoherent radiation source whose radiance is completely independent of viewing angle. The non-Lambertian characteristics of the Spectralon target are removed by the equation provided by Feng allowing and the extended targets to be measured using BuSTeR to be compared against a Lambertian reference to compute the BRDF.

BUSTER has an integrated software package that performs basic data acquisition, data manipulation, motion control, diagnostics and calibration. An overview of the basic tasks includes:

Data acquisition and manipulation programs are required to perform basic input and output through the PXB-1608 and the PXB-241 board, and DMA access for the PXB-1608. The DMA cycle must be synchronized to the new line pulse. Once the data is acquired, software is required for error detection, line averaging, data correction (dark and gain), line alignment, file structure building and storage to disk. Also provided will be the capability to perform statistical analysis on individual pixels, lines or fields of data. The program will have the capability to plot one line of (possibly averaged) data.

Motion control software is supplied to provide basic camera motion control, including camera home position, move to specified coordinates and move during data acquisition.

Diagnostics - The ALU board can be switched into diagnostics mode where it outputs constant values or a ramp. Software is provided to analyze data produced in diagnostics mode, assuring that the system is functioning, synchronized and correctly reading all pixels. The ALU board can also be put into residue only mode, and software is supplied to assure that the output signal is within the range of the A/D converter. The diagnostics include a read loop for the reference photodiode, test loops for motion control, an algorithm to focus the CCD imager, a spectral alignment program and a linearity test.

Calibration software is provided to acquire the raw dark and gain data, compute the calibration terms, including actual reflectance of spectralon for the current solar time, and apply the calibrations to the scanned data.

The BRDF program allows the user to

> scan and plot raw or corrected spectral data
> output SURFER files for 3-D plotting
> apply statistics to scanned data (histogram - mean std dev - view data ...)
> manually read the reference photodiode
> manually control the motors
> read and write to/from all registers
> focus the optics
> apply all systems diagnostics
> impliment DOS commands

Topics covered this section include:

> scanning a line of data
> plotting a spectral line of data
> writing disk files
> basic image statistics
> corrections
> linearity
> focus

The remainder of this section details the overall program package, including menu options, program variables, default setup, and primative functions.

4.1 Menu Options

The BRDF program is setup such that you need not be in any particular menu to impliment a command, menus are for viewer reference only and provide a convenient method for ordering commands. You need only type in enough characters to make the command significant, some commands have names which, at first glance, appear awkward, but only 2 or 3 characters are necessary

to impliment the command. In the following commands list, the least signifigant characters are in bold type.

4.1.1 Statistics Menu

line statistics

Generates mean, std dev, high value , high pixel, low value, low pixel for any one line (n_pixels) of data. This routine is useful for evaluating

* residue level statistics (residue should always be >= 100)
* dark statistics (std dev <= 3)
  a) finds high frequency (pixel to pixel) noise
* data level statistics (full light level <= 16000)

pixel statistics

Generates mean, std dev, high value , high pixel, low value, low pixel for each pixel over an input number of lines. These values are generated for all pixels, and can be viewed 15 pixels at a time starting with an input pixel number. This routine is useful for evaluating line to line noise

histogram

Provides a histogram for a block of data of an input size. Inputs are starting pixel, ending pixel, starting line and ending line. As usual, the program checks for acceptable limits. This option is useful for determining the shape of the noise distribution.

MISC

defaults menu	setup reader defaults parameters (current setting stored in disk file)
return	return to menus menu from any menu
quit program	exits scan program from any menu

BRDF MENU

scan	scan one frame, don't move motors
cycle brdf	execute complete BRDF scan, BRDF stored in BRDF.DAT
brdf slew scan	same as brdf cycle, but 8 scans averaged while slewing
decl cycle	execute declination scan, data stored in brdf.dcl
brdf view	types all λ values for current BRDF point to terminal
time	displays current time and date
suns angle	displays solar time and incident angle

STATISTICS MENU

line statistics	computes mean and std dev for any line in memory
pixel statistics	computes mean and std dev for each pixel over the number of lines in memory
histogram	computes histogram of data in memory
vd view data	view block of data about a given central pixel
error check	assumes smooth spectral data and replaces outlying datapoints with avg of neighbors
peak find	finds peak wavelength and half width for single scan
slope max	finds maximum slope for a single scan

CORRECTIONS MENU

zero dark	load dark corrections buffer with a constant
dark generate	scans dark and generates dark buffer valid for current starting and ending pixels
gain generate	scans gain (manually position spectralon) and generates gain buffer
subtract dark	subtracts dark from image in memory
apply gain	applies gain (including reference reading)
save corrections	save dark and gain buffers to disk (corct.dat)
recall corrections	load dark and gain buffers from values on disk

MOTORS MENU

a motor move	moves declination motor ±n degrees
b motor move	moves sweep motor ±n degrees
delay value	adjust motor speed with motor step delay
power down motors	turn off power to motor windings
home motors	send motors to software home position (0, 180)
exercise motors	moves both motors ±n degrees indefinately
point true south	moves azimuth motor from magnetic south to true south

FILE I/O MENU

write line of data	write one line of (averaged) image data to disk
write brdf file	copies brdf.dat to user named file
read brdf	copies named file to brdf.h
dos command	allows user to impliment dos commands (eg. dir a:)
surfer write	outputs a brdf for a given λ to a SURFER format file

PLOTTING MENU

plot data	plot with X axis as pixels (npix values)
lambda plot	plot with X axis as wavelength (npix values)
brdf plot	same as lambda plot but averaged pixels
plt defaults	display and/or adjust plotting defaults
loop brdf plot	scan and plot loop until any key is struck
hr loop	high resolution scan and plot, refresh screen after 5 lines
saved brdf plot	brdf plot for input declination and azimuth from brdf.dat

DIAGNOSTICS MENU

fill memory	fill allocated memory with specified const
reference loop	read reference photodiode until key is hit
count up diag	test digital path with countup generator on datapath board (dip sw settings prompted)
dc offset	set CCD dc offset (dip sw settings prompted)
focus	adjust CCD height until min peak width (must use 10 nm bandpass filters)
align lambda	adjust Oriel crank until bandpass peak matches system reading
check bad data	scans and error checks for bad data points indefinately

ADDING FUNCTIONS

Functions are easily added to this software package by following three steps:

1) Add menu option to appropriate grouping in menus.c

2) Add to CASE statement in appropriate c program (eg. stats.c)

3) Write software, using available primatives, to perform desired function

DC OFFSET

The analog to digital converter that is used to digitize the output of the CCD has a finite range of -1.25 volts to +1.25 volts. It is very important to have the residue and data outputs from the CCD imager lie within this range so the BRDF option **auto dc offset** is a semi-automatic function which allows the operator set the residue signal within the A/D converter range.

COUNT UP DIAG

The ALU board has an on board pattern generator which can be used to test the digital data path. When this program is run, the operator will be prompted to set the DIP switches on the ALU board, and the pattern generator will substitute a digital ramp for the actual sensor data. The software will automatically check the data for errors.

CCD ALIGNMENT

Two menu options, focus and align lambda, are provided for ccd alignment. Focus is used, in conjunction with the 10 nm bandpass filters, to position the CCD in the focal plane of the monochromator. The three spring loaded allen head bolts are adjusted while the program continually loops displaying the peak value and the full width half maximum value for the filter being used. Align lambda also uses a 10 nm spectral filter, however in this case the operator enters the actual peak wavelength for the filter and adjusts the grating positioning crank until the correct peak value reading is obtained.

The scanner is initialized by setting all switches on the datapath board (BG23 and BG33) to the open position. If other dip switch positions are required for diagnostics, the program will prompt you. Once you are inside the scan program you should make sure the defaults values are as you require. To get into the defaults menu, type **def**aults. Once in the defaults menu, check to see that the following variables are where you want them;

VARIABLE	EXPLANATION
n_rows	# of rows for scan option (max = 32)
lambda_inc	λ averaging / reporting increment (5, 10 or 20 nm)
angle_inc	degrees between BRDF readings (integer)
declination	max BRDF declination angle (90 degrees)
decl_mtr_position	curent position of declination motor (home = 0)
azimuth_mtr_position	curent position of azimuth motor (home = 180)
degrees_true_north	degrees from magnetic north to true north
longitude	local longitude
lattitude	local lattitude
year	year BRDF data acquired (automatically set)
yday	year day BRDF data acquired (automatically set)
hour	solar hour BRDF data acquired (automatically set)
minute	solar minute BRDF data acquired (automatically set)
sun_decl_angle	computed solar declination angle at time of BRDF
sun_azi_angle	computed solar azimuth angle at time of BRDF
sun_inc_angle	computed solar incident angle at time of BRDF
move_mtrs	move motors during BRDF scan? (yes / no)
apply_corrections	automatically apply corrections (yes / no)
use_ref_diode	use reference during corrections (yes / no)

PLOTTING DEFAULT VARIABLES

plot_strtpix	starting pixel to plot (pixel plots)
plot_endpix	ending pixel to plot (pixel plots)
plot_strtlambda	starting wavelength to plot (wavelenght plots)
plot_endlambda	ending wavelength to plot (wavelenght plots)
plot_lowval	min value on y axis
plot_ hival	max value on y axis

The following default variables are autamatically set by the program:

HIDDEN DEFAULT VARIABLES

VARIABLE	EXPLANATIONTION
avg_width	# pixels to average for each λ (2^n)
avg_shift	n from avg_width (# times to shift summed data)
mtr_delay	delay value setting stepper motor speed
print_messages	print messages during scan (yes / no)

The following list explains some of the globally defined constants:

IMG_BASE	base address for DMA access
BASE_1608	PXB-1608 base address
BASE_241	PXB-241 base address
BASE_LAB40	LAB-40 base address
N_PIXELS	total number of raw pixels (1019)
STRT_GOOD_PIX	first usable pixel (3)
END_GOOD_PIX	last usable pixel (916)
TOT_GOOD_PIX	total # of usable pixels (914)
STRT_LAMBDA	first BRDF reporting wavelength (400)
END_LAMBDA	last BRDF reporting wavelength (950)
CAL_OFFSET	wavelength corresponding to first usable pixel (980)
STEPS_PER_DEGREE	stepper motor ratio (160 steps / degree)
BUF_LENGTH	length of globally defined buffers (1024)

The following pointers and / or buffers are used globally:

POINTER	**EXPLANATIONTION**
char huge *byte	huge character pointer to start of framestore
short huge *word	huge integer pointer to start of framestore
long huge *lword	huge long integer pointer to start of framestore
short *dark	pointer to dark corrections buffer
float *gain	pointer to gain corrections buffer
short *line_ptr	pointer to raw data line store buffer
short *brdf	pointer to pixel averaged brdf data line
short *brdf_ptr	pointer to brdf record (all azimuths for 1 declination)
long *line_ave	pointer to buffer used when averaging lines
short *pixel_for_lambda	lookup table mapping pixel number to wavelength

pixel_for_lambda[n] = [cal_offset (n * lambda_inc)] / nm_per_pxl

The following variables are globally defined and used throughout the software package:

GLOBAL VARIABLES

int diode	current reference reading
int diode_dark	stored reference diode dark value
int diode_gain	storedreference diode reading during gain
float nm_per_pixel	system dispersion calibration (slope)
int azimuth	BRDF azimuth reading
int declination	BRDF declination reading
int tot_lambda_pts	total # of spectral readings in BRDF
int tot_decl_pts	tot # of declination angles in BRDF
int tot_azi_pts	tot # of azimuth angles in BRDF
int tot_scans	tot_decl_pts * tot_azi_pts
int tot_record_bytes	total number of bytes in each BRDF record

4.3 Data Acquisition and Manipulation

A typical BRDF cycle might include the following:

declination angles
((90 degrees) / (10 deg/reading) + 1 = 10 readings

azimuth angles
((360 degrees) / (10 deg/reading) = 36 readings

wavelength points
((950 - 400 nm) / (10 nm/reading) + 1 = 56 readings

total brdf bytes
(10 * 36 * 56) readings * 2 bytes / reading = 40 Kbytes

40 Kbytes is quite large, and if 5 degrees per reading or 5 nm per reading settings qre used, a static BRDF buffer becomes too large for the IBM PC. The BRDF program utilizes the hard disk to interactively store and retrieve BRDF

records to a file called BRDF.DAT. Each record contains the complete brdf data for a particular declination angle, including all spectral data for each azimuth point. The data storage format for BRDF.DAT includes a header containing all defaults values, declination reading 0, azimuth reading 0, spectral data, declination reading 0, azimuth reading 1, spectral data, and so on. Cryptically, the data looks like

defaults values (80 bytes)

$D_0\ A_0\ Sp_{00}[56]\ D_0\ A_1\ Sp_{01}[56]\ \ldots\ \ldots D_0\ A_n\ Sp_{0n}[56]$

$D_1\ A_0\ Sp_{10}[56]\ D_1\ A_1\ Sp_{11}[56]\ \ldots\ \ldots D_1\ A_n\ Sp_{1n}[56]$

. . . . . .

. . . . . .

. . . . . .

$D_m\ A_0\ Sp_{m0}[56]\ D_m\ A_1\ Sp_{m1}[56]\ \ldots\ \ldots D_m\ A_n\ Sp_{mn}[56]$

where

D_m = declination reading

A_n = azimuth reading

$Sp_{mn}[56]$ = 56 spectral readings associated with $D_m\ A_n$

Every time a new BRDF is acquired, BRDF.DAT **will be overwritten**. BRDF files can be saved by using the **write b**rdf command while in the BRDF program, or exiting the program and using the DOS "copy" command. Certain functions in the BRDF program (such as surfer write) read brdf data from BRDF.DAT, and any BRDF file can be placed in BRDF.DAT using the **read b**rdf command **w**hile in the BRDF program, or exiting the program and using the DOS "copy" command. Any time the BRDF program reads BRDF.DAT, the **program defaults are reset** to the values stored in the BRDF.DAT header.

PRIMATIVES

get_line(n) located in BRDF.C

retrieves line n from memory and places it into line_ptr[i]

put_line(n) located in BRDF.C

places data in line_ptr[i] into line n in memory

get_lambda_line() located in BRDF.C

pixel averages data (in line_ptr[i]) into desired wavelength increments (5, 10 or 20 nm) and places result in brdf[i]

write_defaults(out) located in BRDF.C

reads the defaults values from disk file pointed to by out (BRDF.DAT) and resets program defaults.

read_defaults(in) located in BRDF.C

reads the defaults values from disk file pointed to by in (BRDF.DAT) and resets program defaults.

get_azi_record(n, in) located in BRDF.C

retrieves the n^{th} azimuth record from disk file (BRDF.DAT) pointed to by in.

put_azi_record(n, out) located in BRDF.C

saves the n^{th} azimuth record to disk file (BRDF.DAT) pointed to by out.

get_brdf_line(n) located in BRDF.C

retrieves the n^{th} brdf record from azimuth record currently in system memory.

fix_data() located in BRDF.C

converts N_PIXELS x N_ROWS of data from raw data stored by hardware to 16 bit signed integers.

solar_incident_angle() located in BRDF.C

creates solar time and date stamp for BRDF file headers and computes solar incident angle for calibrations.

def_read() located in DEFLTS.C

reads default values from def_vars.dat.

def_wr() located in DEFLTS.C

writes default values to def_vars.dat.

set_brdf_size() located in DEFLTS.C

calculates global variables tot_lambda_pts, tot_decl_pts, tot_azi_pts, tot_scans and tot_record_bytes based upon current defaults.

5. Test Results and Analysis

BuSTeR is designed to quantify the reflection characteristics of large (at least 10 meter diameter), reasonably uniform targets under daylight (sunlight and skylight) conditions. The laboratory BRDF system uses a specular illuminator and targets which are less than a foot in diameter, making it difficult to used directly to verify the performance of BuSTeR. The following optical, mechanical and electronic tests have been performed on BuSTeR to quantify systems performance. Many of these tests are located in the diagnostics section of the software, and should be performed periodically to ensure that the system is operating properly.

SIGNAL TO NOISE

Determine RMS noise in the dark for individual pixels.

Determine system response at each wavelength.

Scan and average 32 lines to see if noise averages out after corrections.

RESOLUTION

Spectral response to 10 nm filters.

System linearity at 450, 550 and 650 nanometers.

Reference photodiode linearity.

Quantify polarization effects with and without fiber optic faceplate.

STABILITY

Quantify rise in dark current with temperature.

Repeatability of azimuth and declination moves.

THE INTEGRATED SYSTEM

Acquire full BRDF

Perform azimuth scan through specular reflection angle.

5.1 RMS Noise

One of the first regions of interest for any system which utilizes a CCD imager is the characterization of the dark pattern noise as the ability to make measurements at low levels of radiation is ultimately limited by the dark signal inherent in the instrument detector and amplifiers. The magnitude of the mean dark level is linearly dependent upon the integration time and functionally dependent upon the operating temperature of the imager, and this functionality is thoroughly discussed in the following stability section. There is a pixel-to-pixel pattern in the dark level for this imager, and as the mean dark level rises, so does the RMS value of this pixel-to-pixel variation. The line-to-line variation for individual pixels is indicative of the electronics system noise, and in this system the RMS line-to-line variation is between 3 and 5 A/D counts out of the 16384 counts available for maximum signal. In the 10nm resolution mode, 16 adjacent pixels are summed, reducing the standard deviation by a factor of 4, and the final final RMS variation on the order of 1 A/D count out of 16384 (.0625 counts out of 1000). This line-to-line RMS value has proved to be independent of the limited integration times and operating temperatures encountered on this project. The pixel-to-pixel pattern variation is not a problem, as dark corrections values are generated for each individual pixel, independent of its neighbors, and the pattern is corrected out.

When signal is present, the Poisson noise due to photon collection must be included. The dark noise has Gaussian distribution with a magnitude which is independent of signal level while the photon noise also exhibits a Gaussian distribution however the magnitude varies as the square root of the total signal level (in electrons). Figure 5-0.1 shows the experimentally obtained total RMS noise for a 1.0 reflector. The RMS noise is not spectrally flat because of the multiplication factor used to normalize the nonuniform spectral response discussed in the next section. A reflectorized tungsten source was used for this test (see figure 5-3), resulting in extremely low signal levels below 450 nm and above 800 nm hence prohibiting meaningful data collection in these areas.

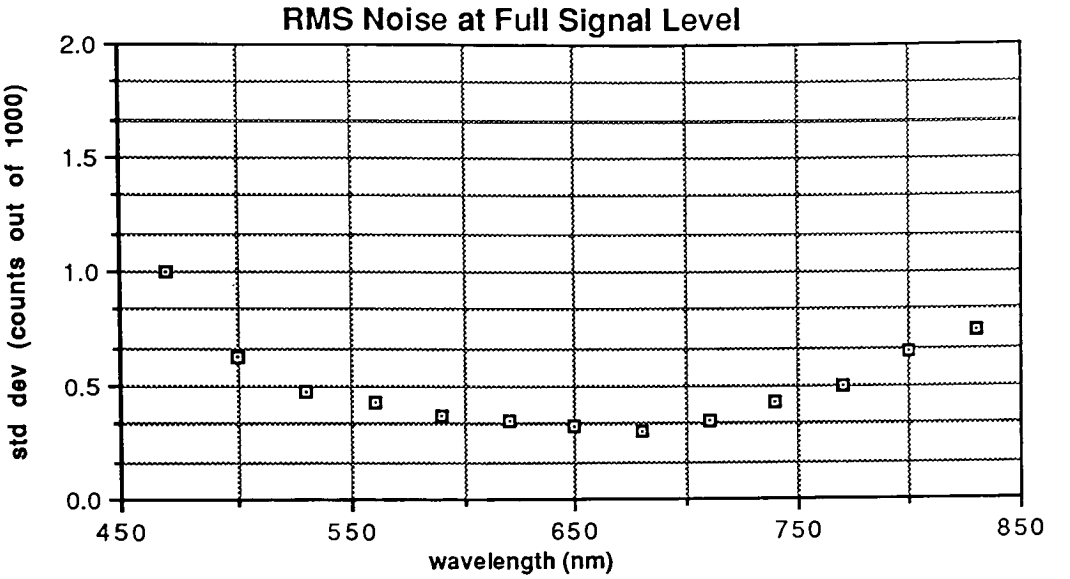

Figure 5-0.1 RMS Noise at Full Signal Level

Since both the dark and photon noise are white noise sources, the total RMS noise level is found by summing the two in quadrature. The CCD imager holds 500,000 electrons at full well and the RMS noise due to photon counting can be modeled by taking the square root of the total number of electrons, dividing this result by the square root of the number of pixels averaged and normalizing to 1000 counts full well. This noise model, which is displayed in figure 5-0.2, compares very favorably to the full well signal noise level displayed in figure 5-0.1 at 650 nm.

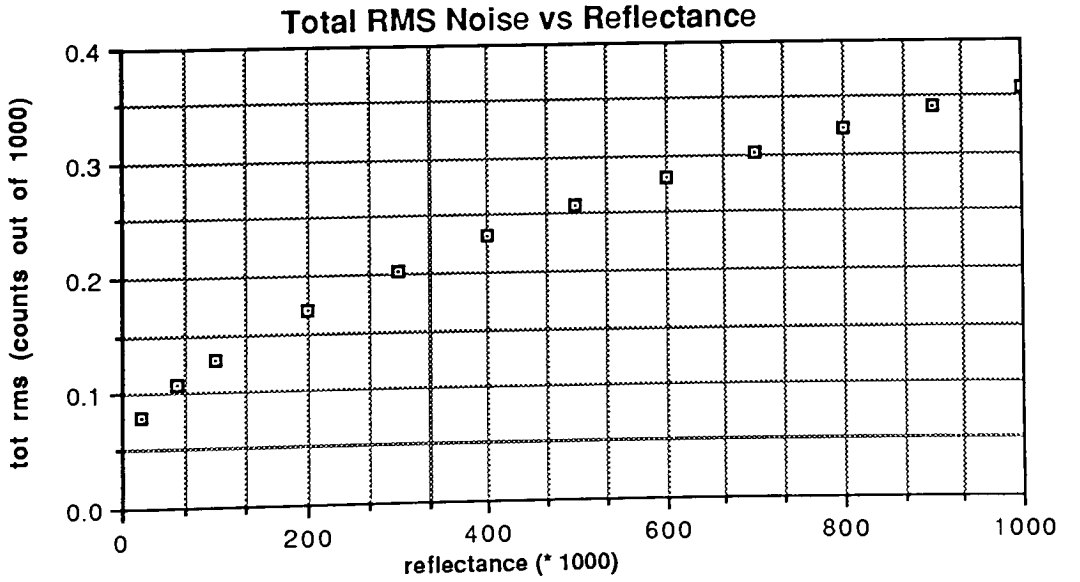

Figure 5-0.2 Total RMS Noise vs Reflectance

The noise model shown in figure 5-0.2 shows that the Poisson noise associated with photon counting is the predominant noise source for anything over a 0.1 reflectance and, since this Poisson noise is signal level dependant, the maximum noise level (maximum uncertainity in reflectance) will occur for the high reflectance case shown in figure 5-0.1. Therefore, the system can measure reflectances to within 0.001 reflectance units.

5.2 Signal

In section the optics section (2.1), the theoretical spectral response of this system is calculated by cascading the spectral response of the CCD imager, diffraction grating efficiency the Kodak Polycontrast PC-2 balance filter transmission and the Kodak Wratten #24 order sorting filter. Figure 5-1 plots the system spectral response using various balance filters and indicates that the PC-2 is the most effective for decreasing the 550 nm peak. Figure 5-2 shows the signal level for the system (with the PC-2 balance filter in place) when viewing a piece of Spectralon (a spectrally flat, Lambertian reflector) during

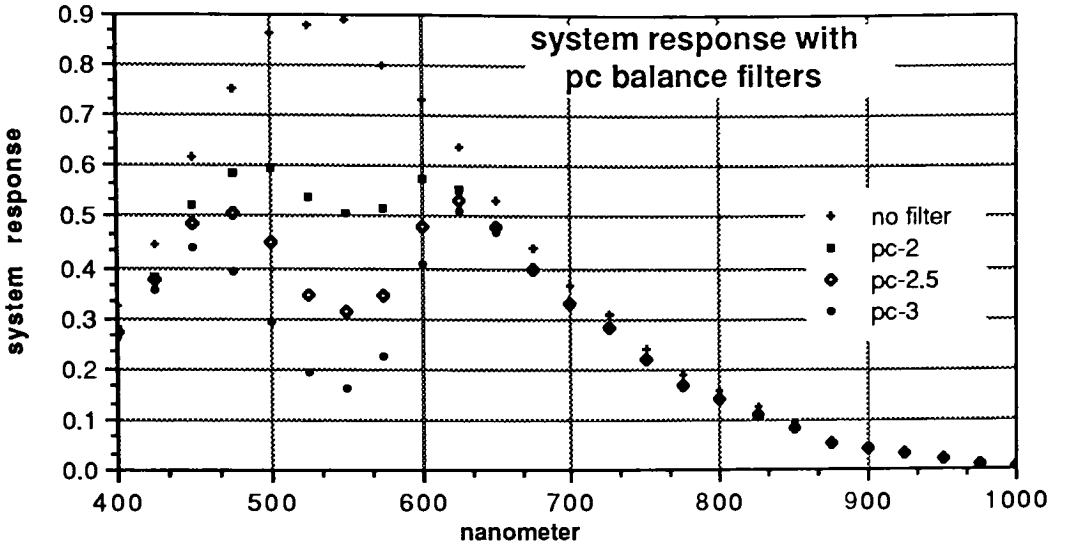

Figure 5-1 Spectral Response

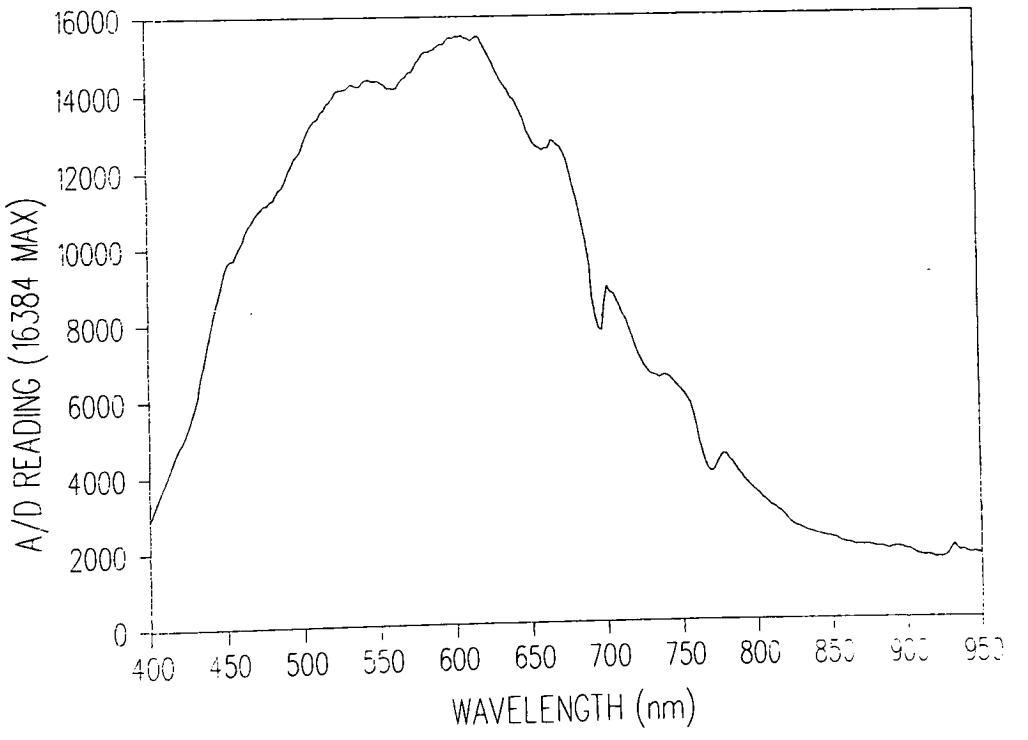

Figure 5-2 Signal in Sunlight

noontime sunlight early in October. The dip at 550nm near the peak of the response is due to the Polycontrast balance filter, and the dip at 700nm is due to the overlap of the balance and order sorting filters. Notice that the rather dramatic shape of the system spectral response results in a maximum signal (at 630nm) to minimum signal ratio (past 850nm) of approximately 8. Figure 5-3 shows the signal level for this system when viewing a piece of Spectralon illuminated by a 42 watt Sylvania TRU-AIM EZY reflectorized tungsten halogen bulb. The reflector coating transmits in the near IR, resulting in virtually no signal above 800nm, and the 3025K tungsten color temperature has substantially less blue light than the 6200K sunlight, resulting in virtually no signal at 400nm.

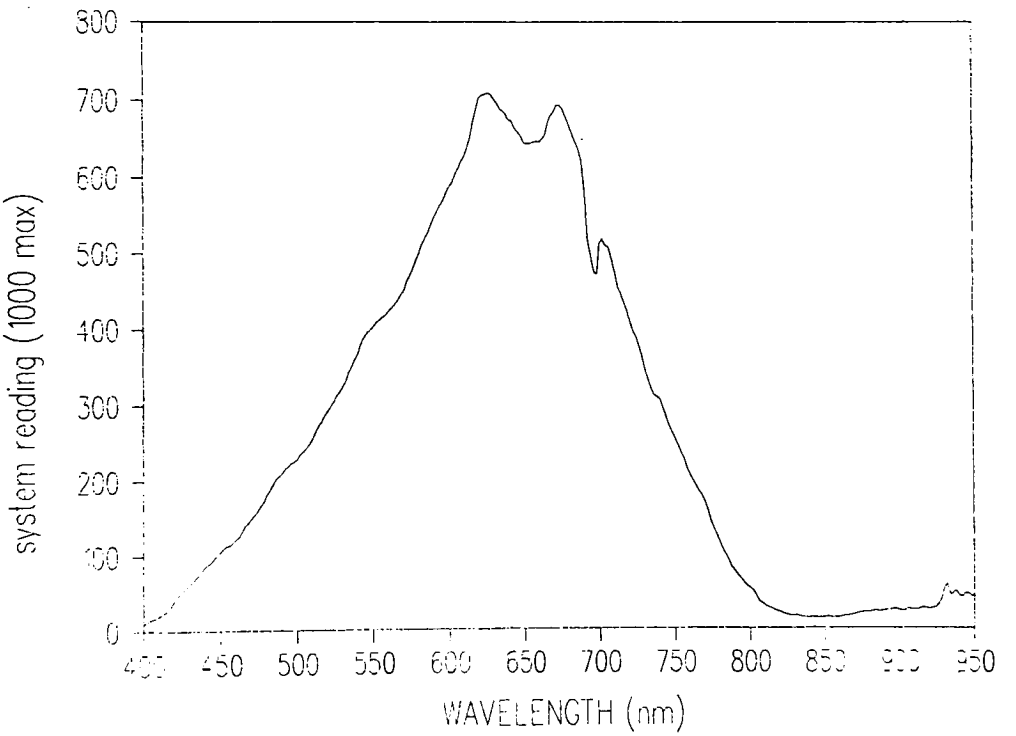

Figure 5-3 Signal With Reflectorized Tungston Source

The shape of the system spectral response results in a poor signal to noise ratio above 800nm in sunlight. Single line scans above 800nm exhibit a peak to peak fluctuation of up to 2%, which can be reduced by a factor of 4 by averaging 16 lines.

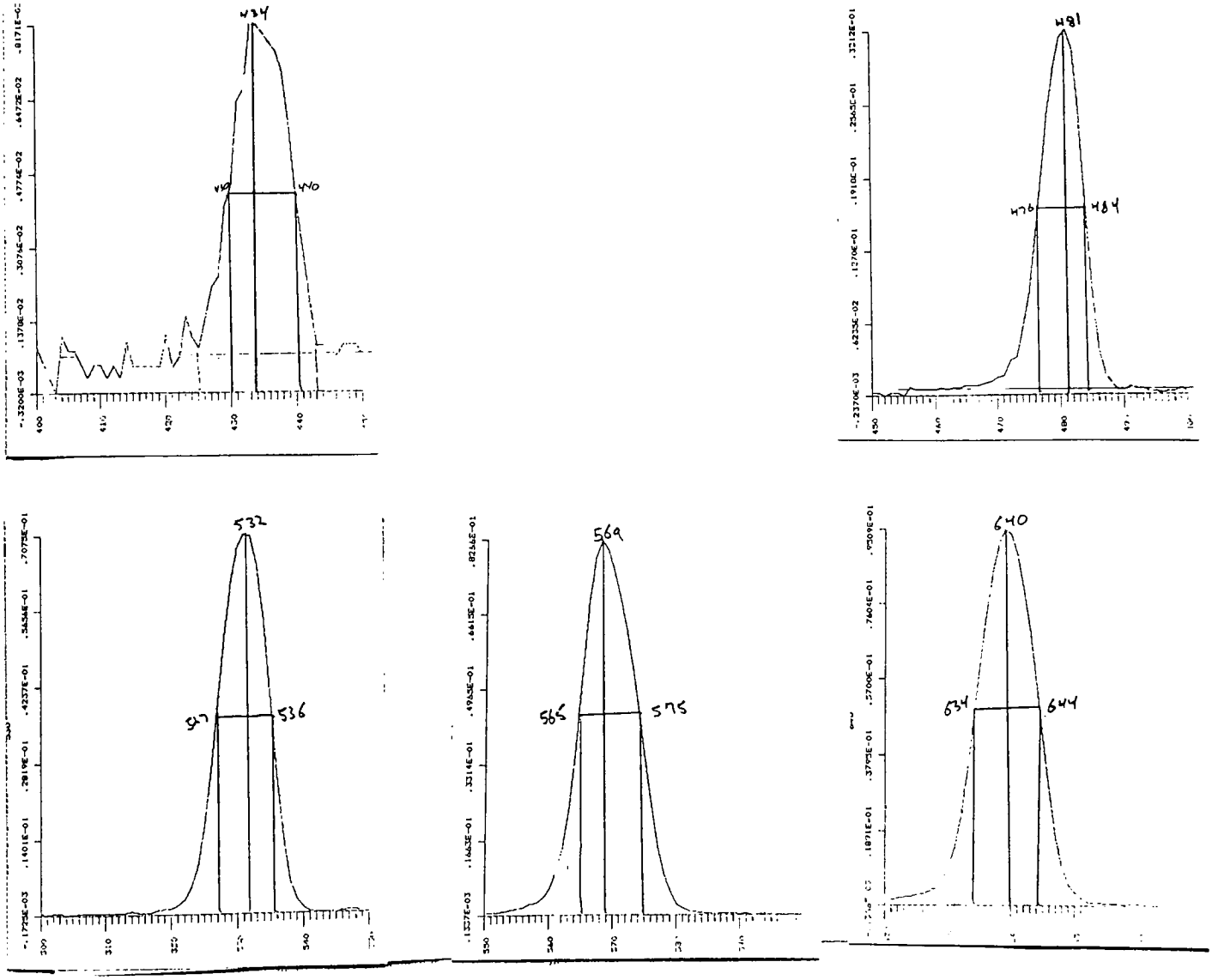

Figure 5-4 Bandpass Filter Transmission Curves

5.3 Spectral resolution

The theoretical spectral resolution of this system is derived in section 2.2, the digital sampling section of this thesis, the essence of which involves convolving the input slit width with the sampling width on the CCD. The actual system spectral resolution was tested by inserting 10nm bandpass filters (figure 5-4) in front of the lens and finding the peak wavelength value and the full width of the reading at the point which is one half of the maximum peak value (FWHM). The results fromBuSTeR are compared against the results obtained from a LI-COR LI-1800 Portable Spectroradiometer operating in the 2nm resolution mode.

Table 5-1 Spectral Resolution

LI-COR LI-1800		**BuSTeR**	
PEAK (nm)	1/2 WIDTH (nm)	PEAK (nm)	1/2 WIDTH (nm)
434	10	434	12
481	8	479	12
532	9	530	13
569	10	569	14
640	10	641	14
668	13	668	16

The peaks obtained by the Field BRDF reflectometer are never more than 2nm away from the peaks found by the LI-COR, and the net effect of the system resolving power has been to widen the 1/2 width by approximately 4nm, which is consistent with the results one obtains by convolving the filter transmission curves with the triangular spectral resolution response function of the system. This test could also have been performed by investigating the known spectral lines of a high-intensity discharge lamp (eg. mercury vapor or sodium).

5.4 Polarization Effects

Diffraction grating efficiency for light which is polarized parallel to the grating grooves is not the same as the grating efficiency for light which is polarized

perpendicular to the grooves. For BuSTeR, light which is polarized horizontally with respect to the ground will be perpendicular to the grating grooves (90^0) while vertically polarized light will be parallel to the groves (0^0). Figure 5-5 shows efficiency curves for two separate gratings, neither one of which is in this system. BuSTeR utilizes an Oriel model #77240 ruled grating which has 400 lines per millimeter and has a blaze angle of 9.2^0 for maximum efficiency at 550nm. Grating efficiency curves for this part are not available, so a test to determine the relative efficiency difference between light polarized parallel and perpendicular to the grating grooves was performed.

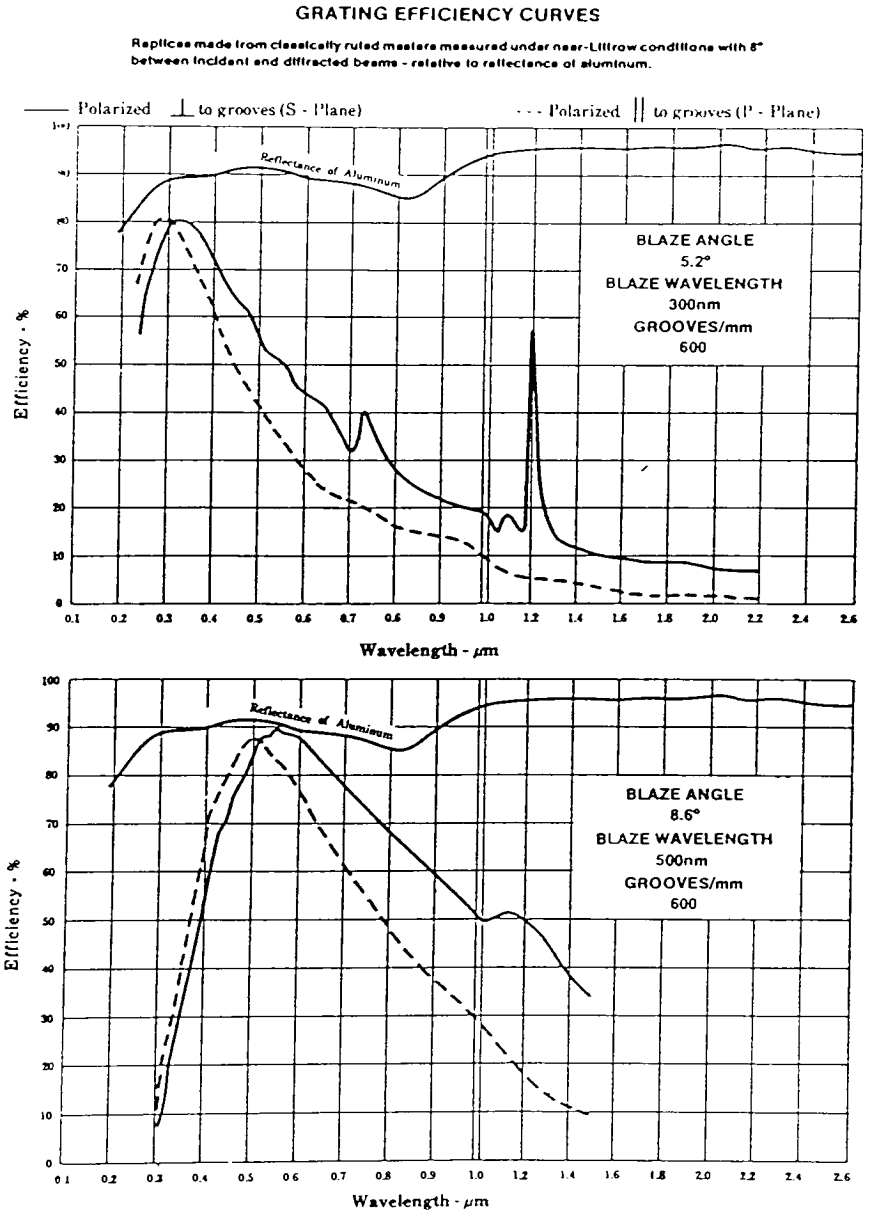

Figure 5-5 Grating Efficiency Curves

The setup for all polarization tests consisted of the reflectorized tungsten source illuminating the Spectralon target at a declination angle of approximately 25^0. BuSTeR was then placed directly above the Spectralon target at a declination angle of 0^0, and the polarizer was placed between the Spectralon target and the reflectometer objective lens. As a check for inherent source polarization, BuSTeR was replaced by the reference photodiode, and no signal difference was detected when the polarizer was rotated between 0^0 and 90^0, indicating that the source is randomly polarized (to 12 bit accuracy).

The relative efficiency difference of the grating for the two polarization states was determined by orienting the polarizer at 0^0 (polarization parallel to the grooves) and acquiring gain corrections values. Next, the polarizer was rotated to 90^0 and a spectral scan was performed and corrected with the stored 0^0 correction values. The results of this test, displayed in figure 5-6, show that not only is there a substantial difference in magnitude between the grating efficiencies, but there are also six distinct spectral peaks.

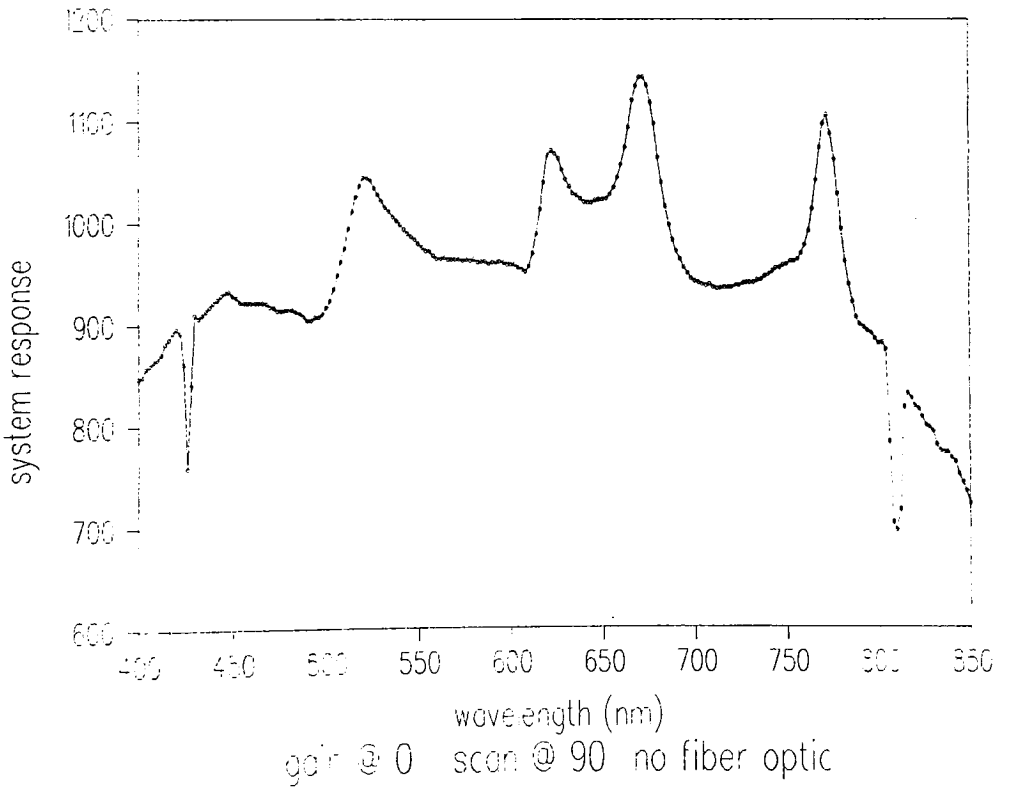

Figure 5-6 Relative Polarization Response of Grating

The magnitude of the error indicated by this plot is actually much greater than that which would be found in practice, as the correction reference data will always be acquired from the sun illuminating the Spectralon target, and hence randomly polarized. In an attempt to model the worst case scenario, the gain corrections were acquired with the polarizer at 45^0, causing both parallel and perpendicular polarization angles to contribute equally to the corrections terms, just as they do in the randomly polarized case. Next, scans were performed at 0^0 and 90^0, and corrected against the 45^0 case. The results of this test are displayed in figures 5-7 and 5-8. Note that these two graphs are virtually mirror images of each other with the possible exception of wavelengths less than 420nm or greater than 800nm, where lack of signal from the reflectorized tungsten source inhibits us from determining the system response in these areas.

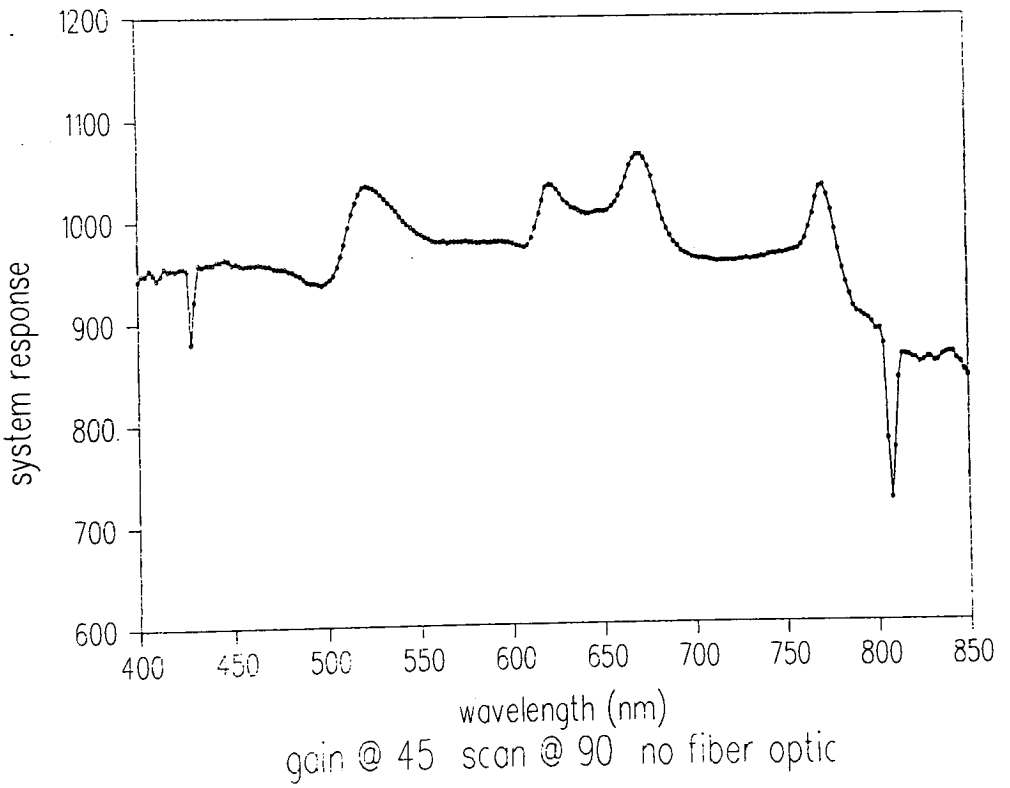

Figure 5-7 Relative Polarization Response of Grating

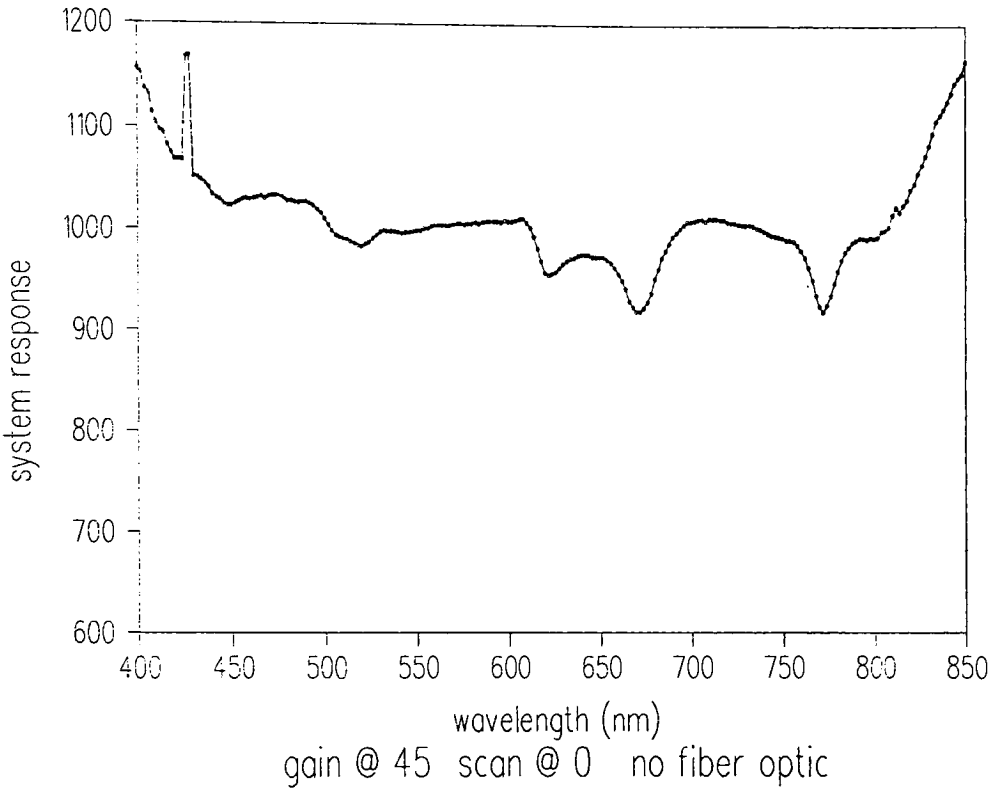

Figure 5-8 Relative Polarization Response of Grating

As mentioned in the Optics section of this thesis, a 0.25" long fiber optic faceplate with 0.002" diameter fibers is used in the system in an attempt to randomize any polarization preference. The normalized data presented in figure 5-9 was acquired by placing two linear polarizers between tha tungsten source and the LI-COR spectraradiometer. One of the linear polarizers remained stationary while the other was rotated and, as the plot shows, when the fiber optic faceplate was inserted between the two polarizers approximately 65% of the polarized light remained polarized.

This same experiment was performed by placing a 24 inch long fiber optic bundle between the two polarized, and in this case was no no signal difference between the 0 and 90 degree relative polarizer angles. I have no other fiber

bundle lengths to experiment with, but these results show that the 0.25" fiber optic faceplat is 35% efficient while a 24" long bundle is 100% efficient.

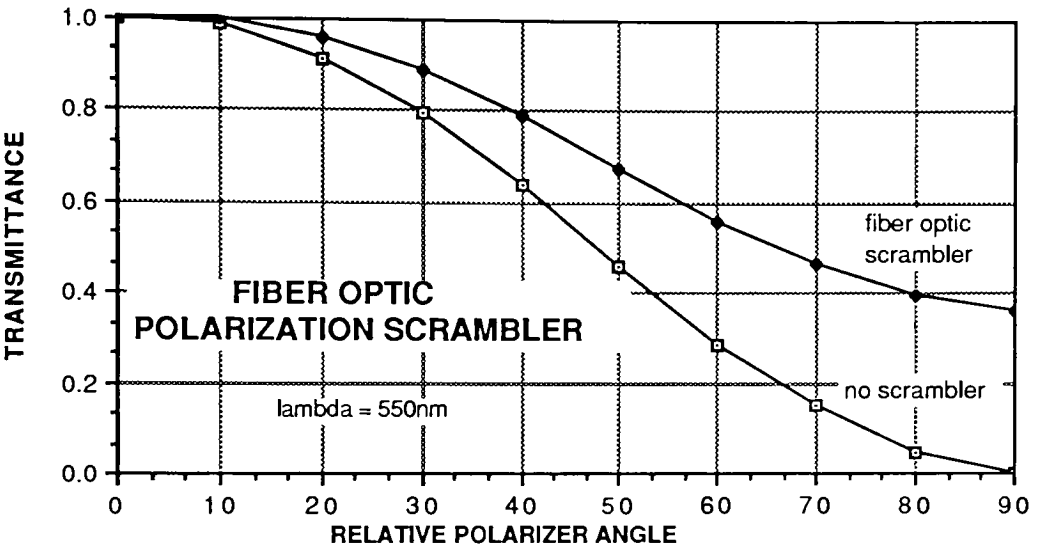

Figure 5-9 Fiber Optic Polarization Scrambler Effiency

The real test is to insert the fiber optic faceplate into the reflectometer and quantify the scrambling effects in the actual system. First, with no fiber optic faceplate in the system, gain correction values acquired with the polarizer positioned at 45^0, then data was acquired for polarizer angles between 0^0 and 90^0 at 5^0 increments, and corrected with the 45^0 corrections data. Next, the fiber optic faceplate was inserted into the reflectometer and the correction / data acquisition cycle was repeated. The results are displayed in figures 5-10 and 5-11, which show that fiber optic faceplate reduces polarization effects by approximately 30%, which is consistent with the results obtained in the crossed polarizer test.

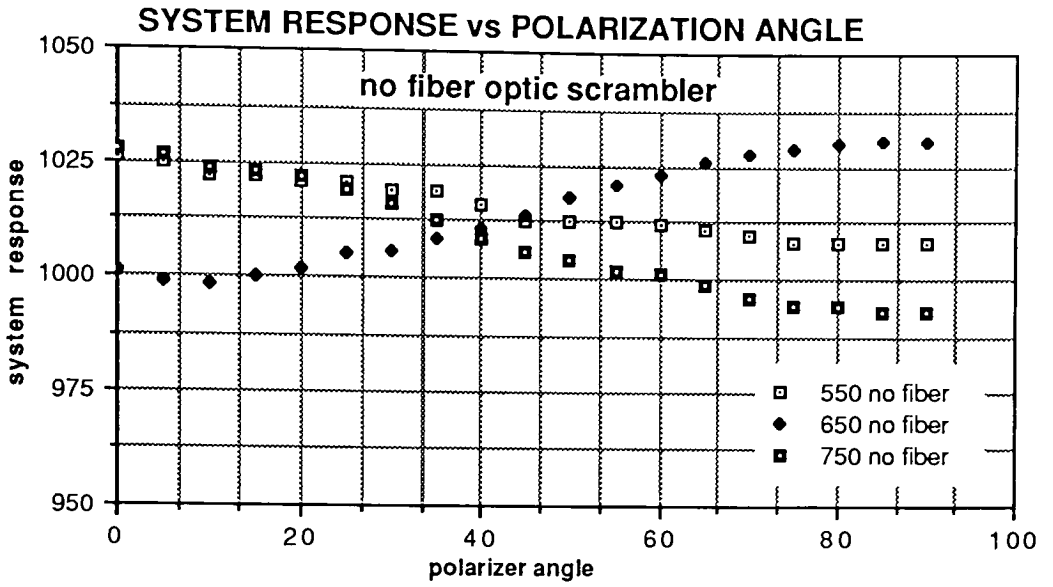

Figure 5-10 Polarization Effects Without Fiber Optic Faceplate

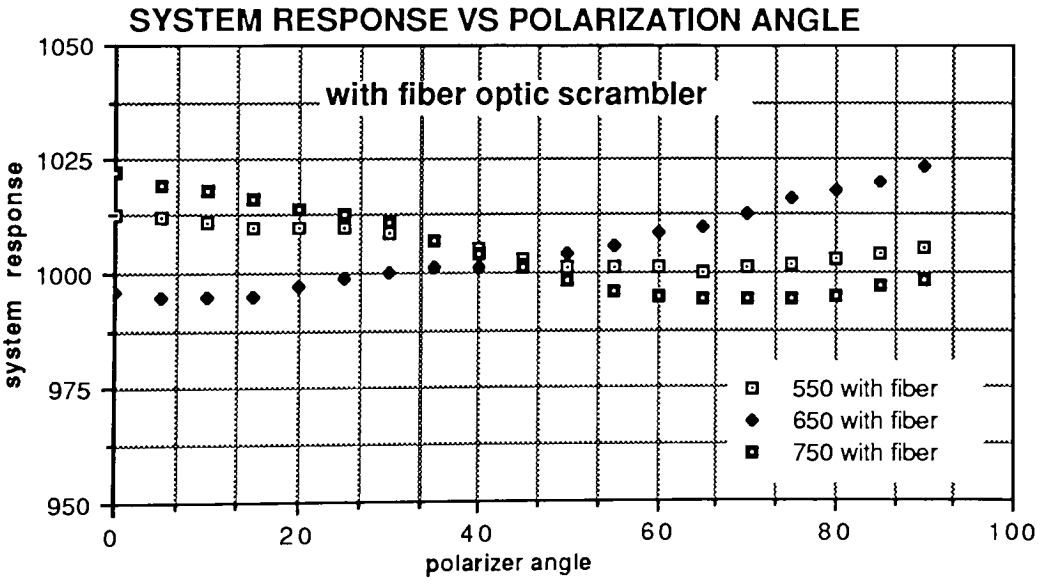

Figure 5 11 Polarization Effects With Fiber Optic Faceplate

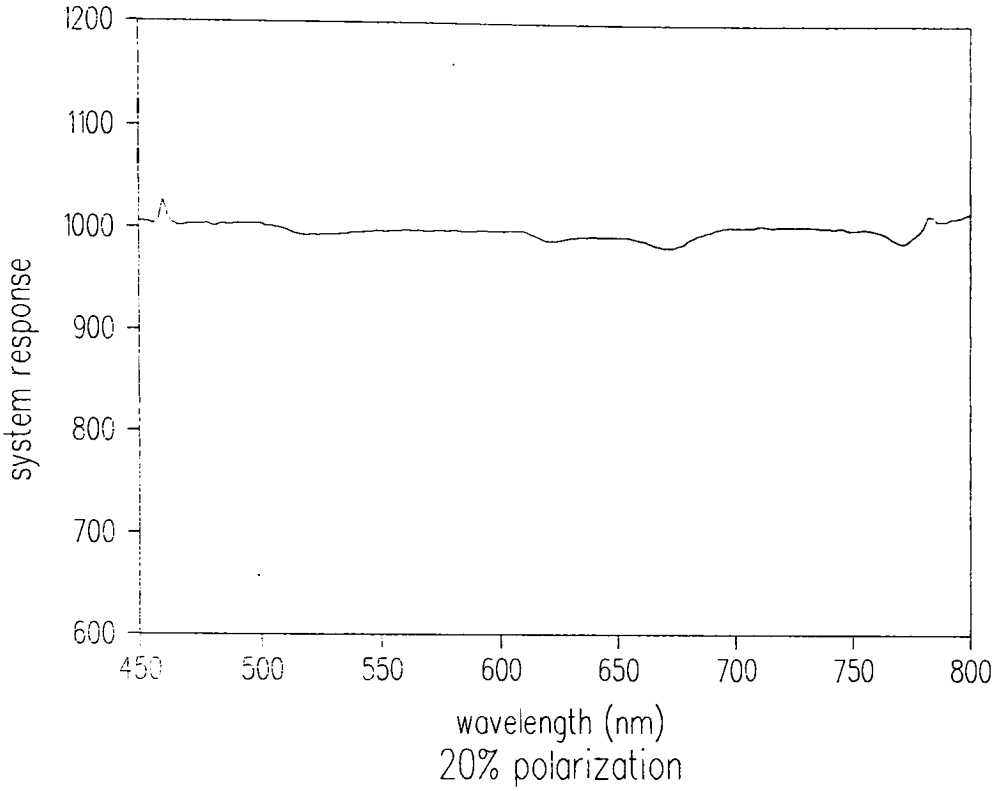

Figure 5-12 Effects of 20% Polarization With Fiber Optic Faceplate

Figure 5-12 shows that, with the fiber optic faceplate in place, there is a maximum error of ±2% for 20% linear polarized light, which covers the majority of mineral and vegetation reflective characteristics (Egan, 1988). In fact, the light reflected by a leaf consists of two components (Coulson, 1989). First, a part of the incident light is reflected by the wax cuticle and other material at the surface of the leaf without entering the main body of the cellular structure. This type of largely specular reflection is primarily responsible for the polarized content of the reflected light (Vanderbilt, 1985). The second component of the incident light enters the leaf structure, and may be either transmitted, absorbed, or reflected. The reflection in this case is diffuse in nature, and the diffuse light is mainly unpolarized. So, polarization effects due to a nonuniform grating efficiency will not be a problem except at specular reflectance angles. Even for specular reflectance (well away from the Brewster angle), the polarized component of the light will be low, and the effects will be minimal.

5.5 Linearity

The linearity of the reflectometer was tested by using the same experimental setup described above in the polarization, except the polarizer was replaced with precision metallic neutral density (ND) filters. The actual densities of the filters at 450nm, 550nm and 650nm were recorded and compared against the system readings with the appropriate filter in place. The density reading is the $\log_{10}$ of the ratio of the transmission reading without the filter in place to the transmission reading with the filter in place. The results of this test are displayed in figures 5-13, 5-14 and 5-15, and these figures indicate that the system response is linear, within the limits of experimental accuracy, over a density range of 2.

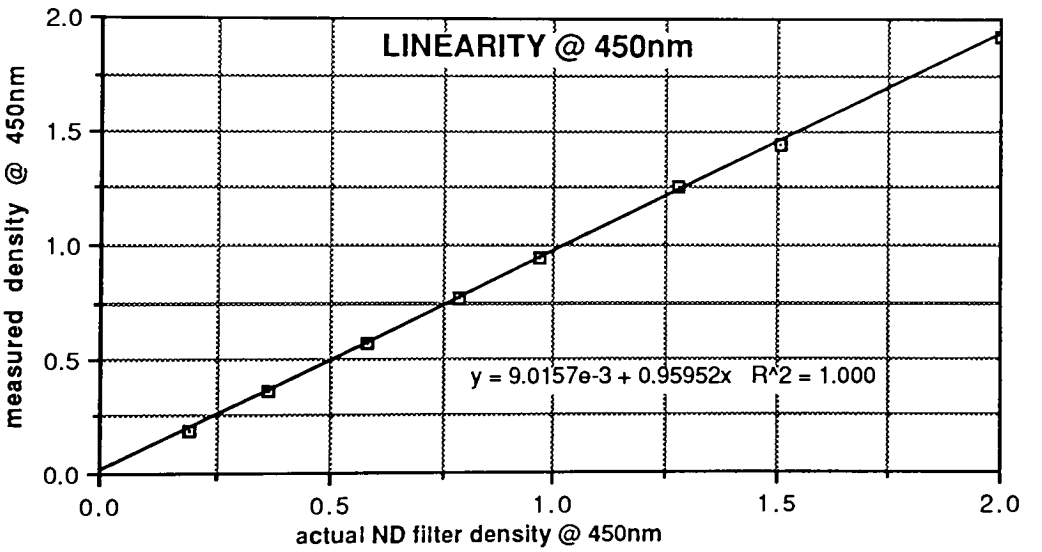

Figure 5-13 System Linearity at 450 nm

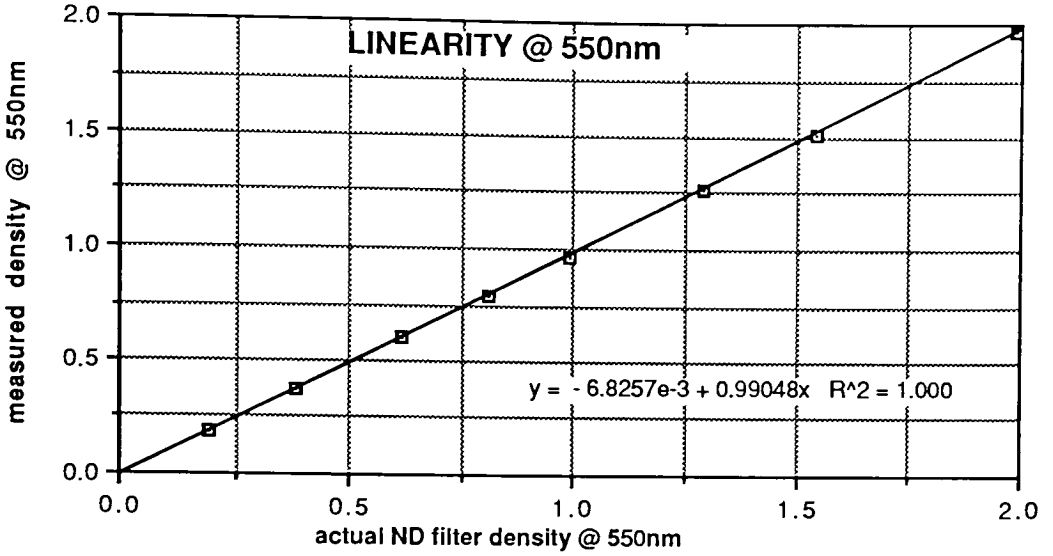

Figure 5-14 System Linearity at 550 nm

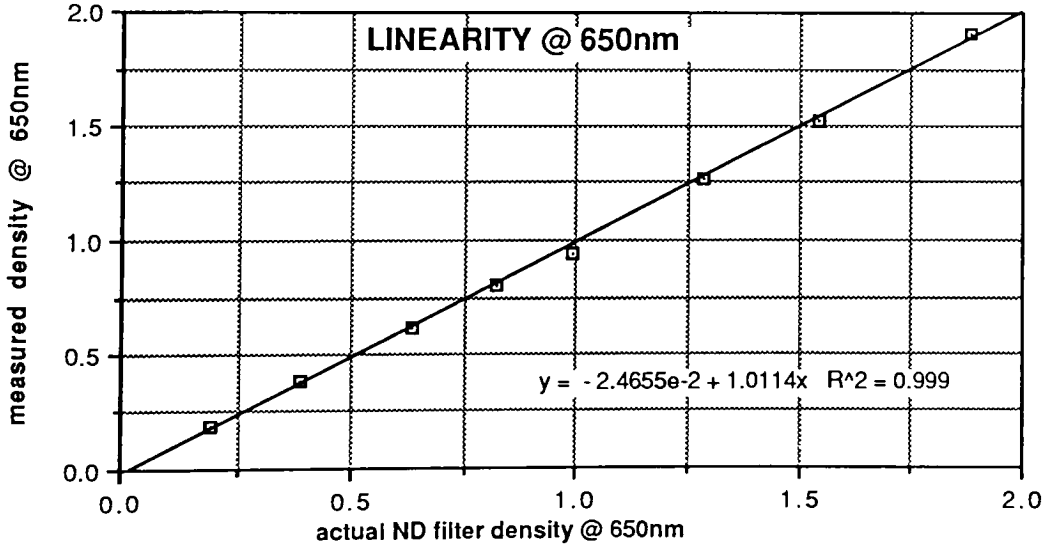

Figure 5-15 System Linearity at 650 nm

Figure 5-16 shows that the reference photodiode response is linear over a density range of 1. Since the purpose of the reference photodiode is to compensate for minor changes in the source, the operating range of the reference photodiode will be very limited.

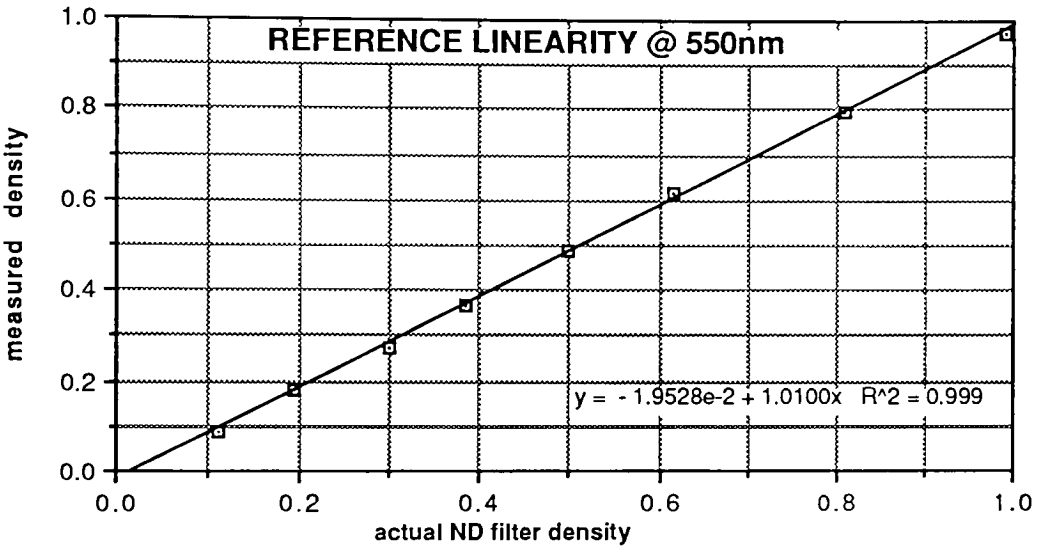

Figure 5-16 Reference Photodiode Linearity at 550 nm

5.6 System Stability and Repeatability

The mechanical repeatability of this system is dependent upon the ability of the stepper motors to accurately perform repeated moves. An underpowered stepper is likely to miss steps or stall, so a test was developed to move the motors ±n degrees repeatedly, and the positional graduations on the alt-azimuth positioner are used to insure that the correct endpoints are always obtained. The azimuth motor occasionally misses steps at speeds greater than 1.7 degrees per second (motor delay value = 800), and the declination motor is unreliable at any speed. The problem with this drive system is not the motors, as they are rated for torque values which are more than enough for this application. Due to funding considerations, a LAB-40 stepper controller was purchased (approximately $100) and this board simply cannot source the current necessary to realize the potential positioning speed and repeatability of these motors. The temporary solution implemented for the completion of this thesis has been to position the declination angle by hand and run the azimuth motor approximately a factor of 10 slower than the desired speed. A complete BRDF data acquisition cycle should, for reasons to be mentioned in the next few paragraphs, take no longer than 5 minutes.

The dark and gain corrections are used to null out any system nonuniformities and provide accurate BRDF readings at each wavelength. The spectral response of this reflectometer (figure 5-2) indicates that the gain corrections will not be uniform, in fact they will be proportional to the inverse of figure 5-2. Since the gain corrections terms are not spectrally uniform, any dc shifts in the signal from source fluctuations or changing dark current will cause a nonuniform shift in the system output, weighted most heavily at in the deep blue and near IR.

The reference photodiode is intended to compensate for any source (solar) fluctuations, and the photodiode response has proven to be stable and linear (figure 5-15). The best results are obtained by pointing the photodiode at a diffuse white reflecting surface, such as Halon or Spectralon, to minimize the effects of solar movement during long BRDF data acquisition cycles.

The magnitude of the dark current is functionally dependent upon the operating temperature of the CCD imager. The optical and front end electronic components are mounted to the same base plate (which is mounted to the positioning system), and the entire front end is enclosed to keep stray light away from the CCD imager. This arrangement worked fine for all of the indoor tests, but once the system was taken outside for real BRDF scans, the temperature inside the enclosure rose continuously. After 2 to 3 hours of use, it was not uncommon to have mean dark readings in excess of 1200 counts (with a 52 millisecond integration time). System performance here is also degraded by long data acquisition cycles which give the system more time to drift away from the operating parameters in effect at the acquisition time of the corrections.

Figure 5-17 shows the effect of dark current drift on BRDF readings. The plots on this graph represent corrected reflectance readings from a piece of Spectralon immediately after acquiring corrections (0 minutes), 5 minutes after corrections and finally 20 minutes after corrections. The addition of a strong

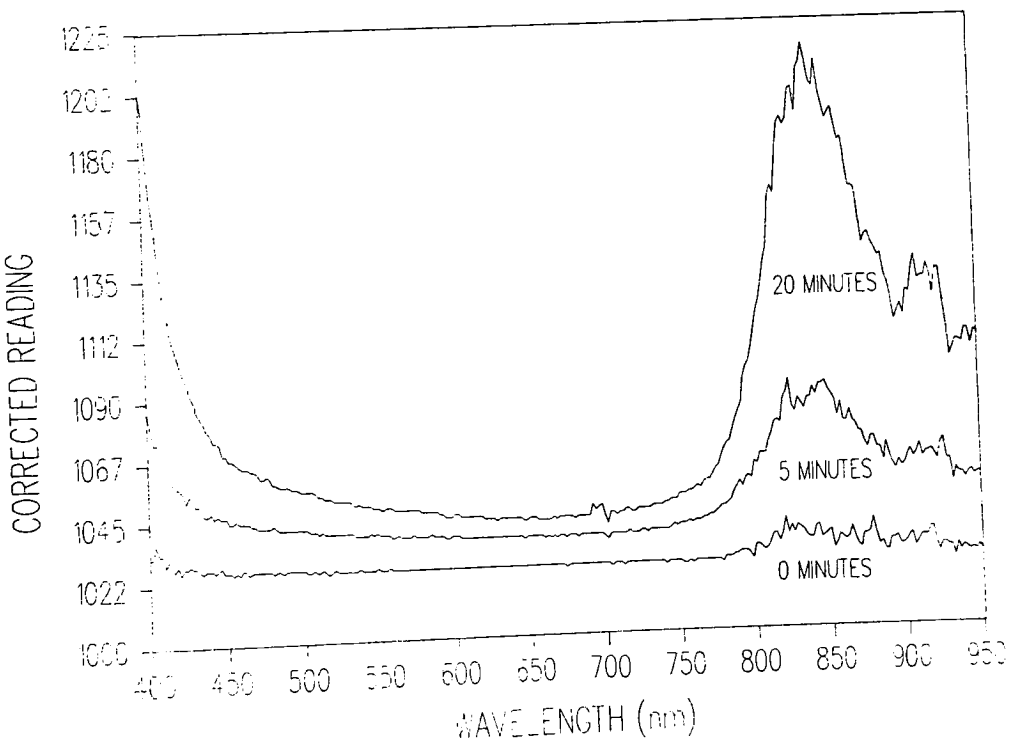

Figure 5-17 Signal Effects from Dark Current Drift

muffin fan which blows air into the enclosed opto-electronic head has virtually eliminated the dark drift problem. Stability tests over a period of three hours have shown that, after a 10 to 15 minute warmup period, the mean dark current value will not change unless the ambient temperature outside changes.

A temperature sensor was affixed to the CCD imager and figure 5-18 shows a plot of the dark current readings at various operating temperatures (with a 52 millisecond integration time).

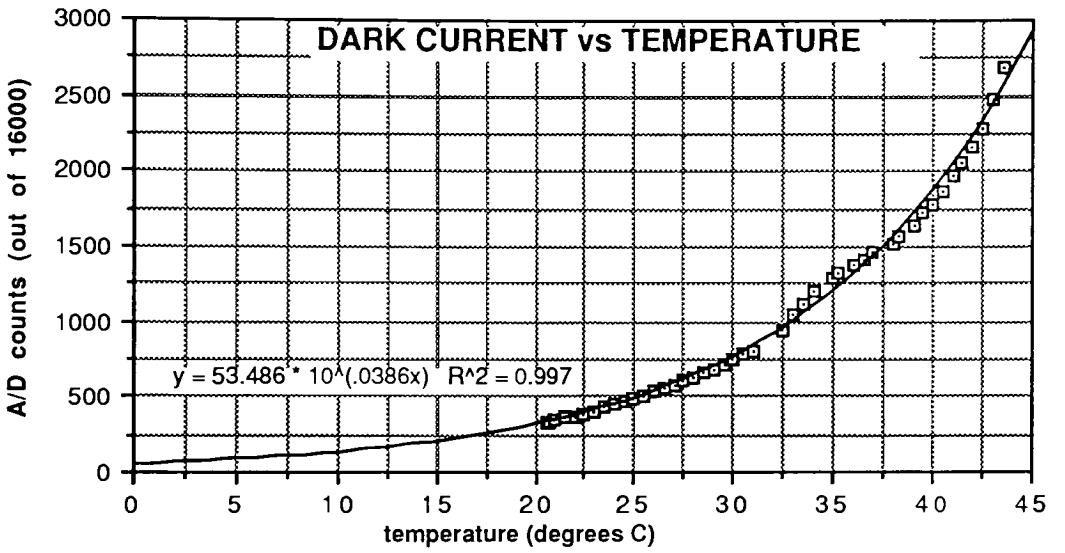

Figure 5-18 Dark Current vs Temperature

The graphics package used fit a curve of

$$y = 53.486 * 10^{0.0386t}$$

The Toshiba CCD image sensor data book claims that the mean dark current will double with each 8°C rise in temperature, or

$$y = y_o * 2^{t/8}$$

$$\log_{10} y = \log_{10} (y_o * 2^{t/8}) = \log_{10} y_o + \log_{10} (2^{t/8})$$

or

$$\log_{10} y = t/8 \log_{10} 2 + \log_{10} y_o = 0.0376t + \log_{10} y_o$$

and finally

$$y = y_o \, 10^{0.0376t}$$

which is good agreement with the experimentally derived result.

As mentioned earlier, target uniformity makes it very difficult to quantitatively compare results from this system, which obtains each data point from a physically different point, to the results of a laboratory system which repeatedly using a 6" target. The above mentioned tests prove that BuSTeR is linear and stable with 10 nm spectral resolution and the positioning mechanics is designed to provide better than a 0.01° positioning resolution. Given these basic attributes, the system will provide accurate BRDF measurements for unpolarized reflections.

A large target was fabricated out of a 6 foot by 8 foot blue-green piece of indoor outdoor carpeting. Figure 5-19 shows a spectral plot of the results of a declination angle scan at the fixed azimuth which would result in specular reflections. Notice that there are two distinct spectral peaks, the blue-green peak at 490 nm and another peak in the near IR at 800 nm. The data acquisition cycle was slightly flawed at -60 degrees (I manually positioned the declination wrong), so ignore that data point. The dip at -20 degrees is due to shadows from the camera head and tripod.

Figures 5-20 thru 5-23 are 0 to 40 degree declination by 360 degree azimuth BRDF plots (in 10 degree increments) of the 6' by 8' carpet for 550nm, 650 nm, 750 nm and 850 nm respectively. The carpet is not quite large enough for a full BRDF scan, and the camera occasionally pointed at areas which were off the carpet. The azimuth positions most susceptible to missing the target are at the endpoints of the 180 degree sweep, 80° and 260°. This data was acquired at approximately 11:00 AM on November 3, which was a rather windy day with fairly substantial cirrus cloud cover. The wind was blowing leaves across my target, which may or may not have affected the readings.

Figure 5-24 is a declination plot of the parking lot behind the Imaging Science building at RIT. Once again, only the declination angle is changed and the equipment is set up so that the sun is in the declination plane. This data was acquired at shortly after noon late in November, and the declination angle of the sun was approximately 59° Notice that the parking lot spectrally flat and is much more Lambertian than the rug. There is a gradual rise between -40° and -60° due to specular backscattering and a very strong peak at +60° due to specular reflection of the incoming solar radiation.

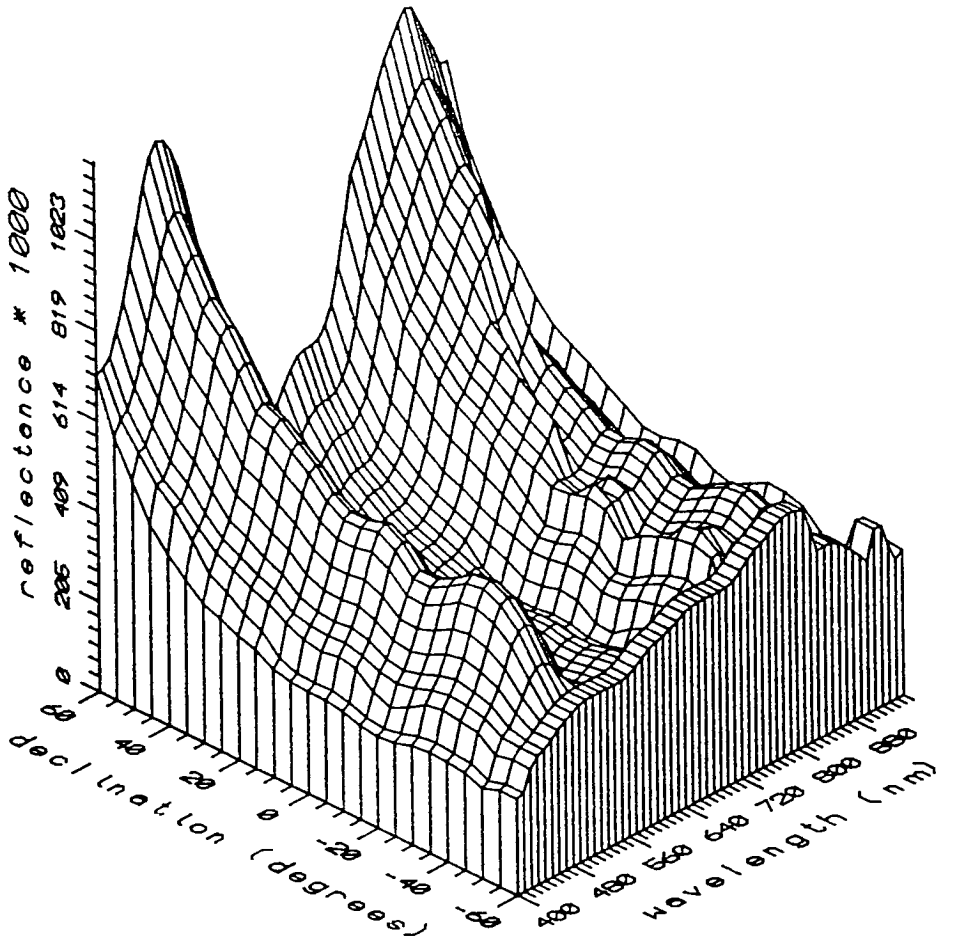

Figure 5-19 Spectral Data from Declination Scan

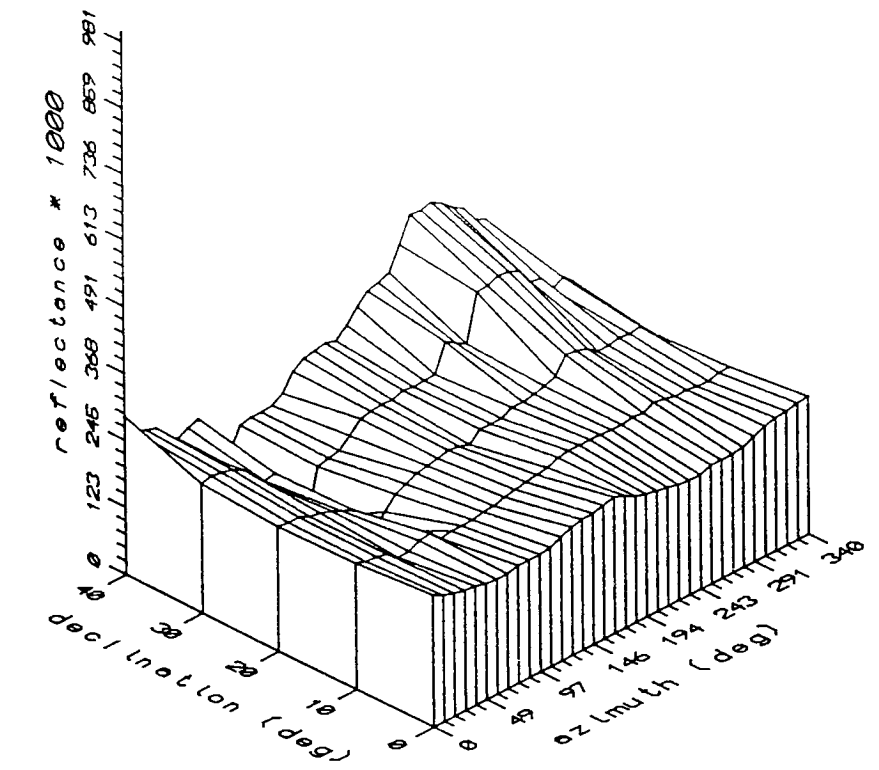

Figure 5-20 Rug BRDF at 550 nm

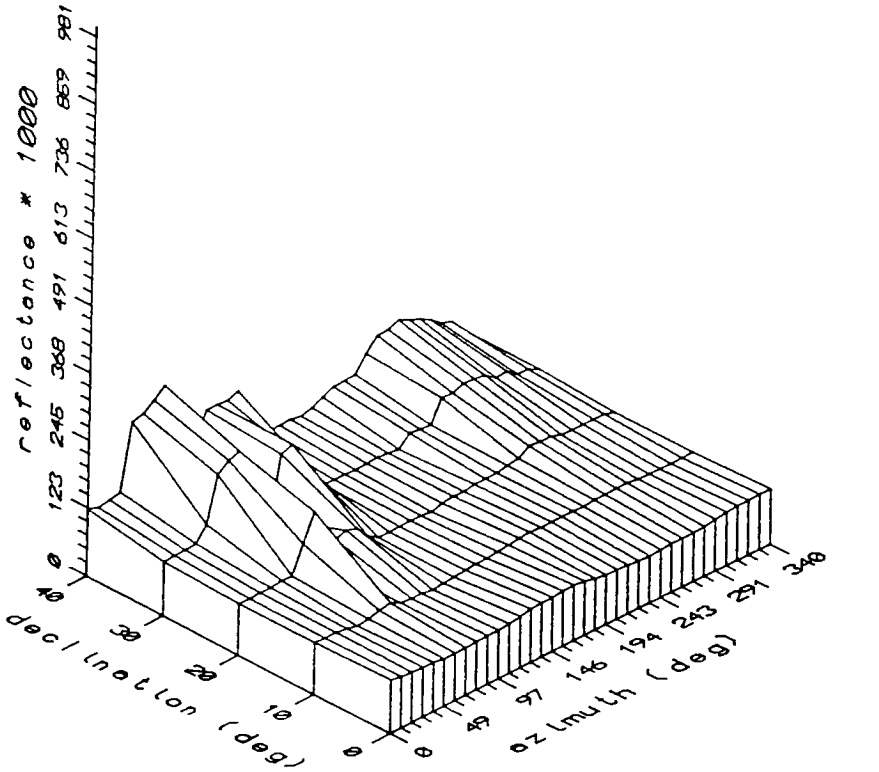

Figure 5-21 Rug BRDF at 650 nm

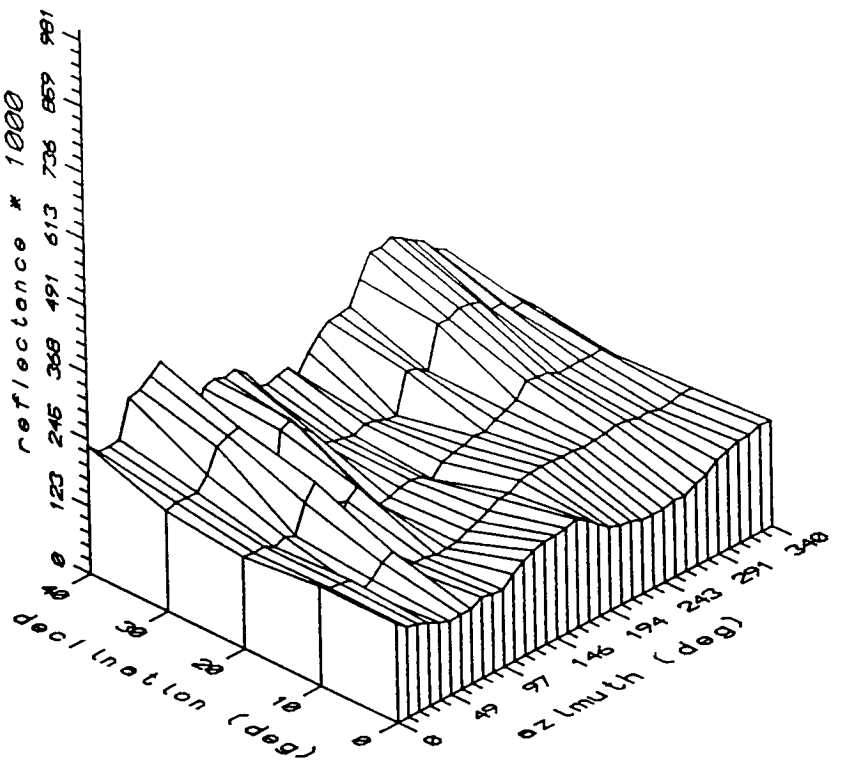

Figure 5-22 Rug BRDF at 750 nm

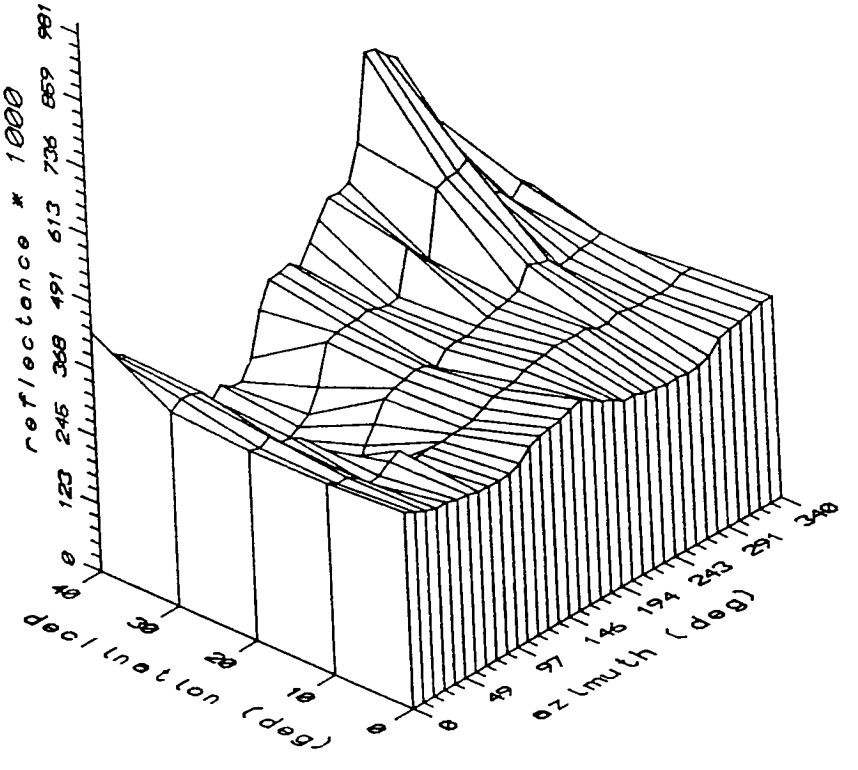

Figure 5-23 Rug BRDF at 850 nm

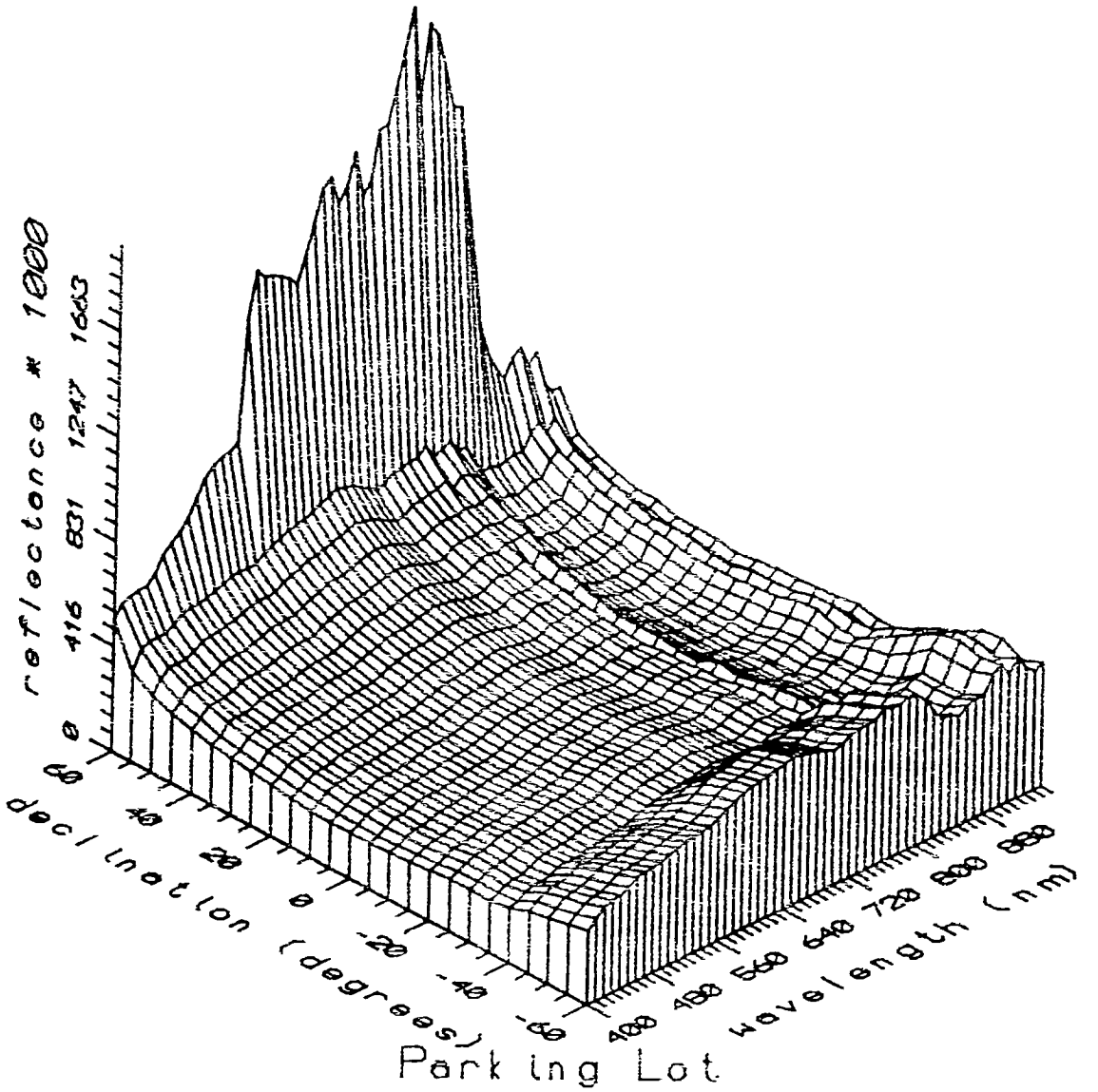

Figure 5-24 Declination scan of a Parking Lot

6. Areas for Improvement

There are four aspects of this device which either limit or degrade the systems performance, namely positioning motor performance, narrow field of view, low spectral response in the near IR and polarization dependence. These three limitations are discussed here with recommendations for improvements.

6.1 Drive System

The most limiting factor in this piece of equipment is the stepper motor translator used to drive the declination and azimuth positioning stepper motors. As mentioned in the systems tests section, the declination motor is not capable of positioning the opto-electronic head, and this axis must be hand positioned. The azimuth motor is functional if it is operated under 1.7 degrees per second, or 270 steps per second. As mentioned earlier, the problem here is not that the motors are too small, as the Superior Electric M061-FD02 5 volt 1 amp motor is rated for 35 ounce inches of torque, which is more than enough for this application. The LAB-40 system purchased to control the stepper motors consists of two components. The first component is the LAB-40 generator, which is the interface card that resides in the PC backplane and is used to send TTL level pulses to the LAB-40-5 Four Axis Stepper Drive Module, the second component which supplies the four step input sequence and current required to move the motors. The is the LAB-40-5 is the weak link in this system, as it cannot source the current necessary to realize the potential torque and positioning speed of the MO61 stepper motor.

Superior Electric manufactures a complete range of translators and preset indexers capable of stepping rates from 1000 to 10000 steps per second. A translator converts TTL pulses from an external source (eg. LAB-40) into the switching and sequencing logic for bidirectional control of a stepping motor, making it the ideal solution requiring little or no software changes. Probably the two most promising prospects are the SLO-SYN STM 101 1000 step per second

or the SLO-SYN STM 103 3000 step per second translator module ($220 and $350 respectively). The 3000 step per second module would be most desirable, providing a factor of 10 increase in positioning speed.

A longer range solution which would allow the system to perform other tasks (signal averaging, corrections, etc.) while the motors are moving would be to use preset indexers, which are loaded with a move parameter and then execute that move. This change, however, would require more extensive (but not prohibitive) software modifications.

6.2 Field of View

The narrow field of view of this system is a direct result of the size of the photosites in the CCD array. The imager in this system was picked because it was available with all necessary electronics including drive clocks, A/D converter, correlated double sampling circuitry and pixel summing circuitry. The imager, however, is designed for imaging applications and, as a result, has a large number (3648) of very small photosites (8 μm x 8 μm). Photosites are summed together and cylindrical optics are used in an attempt to increase the field of view, but the optimum solution is to use an imager which is designed for spectroradiometric applications. The optimum sensor would have 110 photosites, each of which has dimensions of 0.5 mm x 0.5 mm on 0.5 mm centers, providing a square 1.4 degree field of view (and an increased signal level as well).

6.3 Spectral Response

As mentioned above in section 6.2, The Toshiba TCD 105C imager was designed for imaging applications. The use of the microdefect wafer and p-Well structures suppress sensitivity to long wavelengths of light, which is good for color imaging applications but bad for near IR performance in our application. Figure

2-7 shows that both the Image sensor spectral response and the grating efficiency peak at approximately 550 nm. The optimum solution to the poor near IR performance is to, once again, purchase an imager which is designed for spectroradiometric applications, however, a custom grating which is blazed for maximum efficiency at 800 nm would increase the spectral response in the near IR.

6.4 Polarization Dependence

The fiber optic faceplate used to randomize the polarization state of the light entering the optical system was designed to be 0.25" thick for two reasons. The first reason was to minimize the impact on the existing input features on the Oriel 7240 monochromator. The resources available for this project were very minimal, and radical redesign efforts were not practical. The second reason for choosing a 0.25" thick faceplate is the rule of thumb, which turned out to be an old wives tale, stating that a fiber which is 20 times as long as its diameter will randomize the polarization state of the light transmitted. The fibers are 0.002" in diameter, hence 125 times as long as the diameter, and this faceplate is 30% efficient at randomizing the polarization. The simplest solution to the polarization dependence is to purchase a thicker fiber optic faceplate (1" - 2") and modify the monochromator to accommodate the larger faceplate.

7. References

1. D.W. Deering, P. Leone, "A sphere scanning radiometer for rapid directional measurements of sky and ground radiance", Remote Sensing Environment, **19**, 1-24 (1986)

2. B.F. Robinson et. al., "Performance evaluation and calibration of a modular multiband radiometer for remote sensing field research", Proc. SPIE **308** 146-157 (1981)

3. D.W. Deering, "PARABOLA Directional Field Radiometer for Aiding in Space Sensor Data Interpretations", Proc. SPIE 9**24** 249-261 (1988)

4. R.D. Jackson et.al., "Field Calibration of Reference Reflectance Panels", Remote Sensing Environment, **22**, 145-158 (1987)

5. T.M. Lillesand, R.W. Kiefer, Remote Sensing and Image Interpretation, John Wiley and Sons, New York, New York (1987)

6. J.R. Schott, Remote Sensing Lecture Notes, (1988)

7. V.C. Vanderbilt et.al., "Integrating sphere transmissometer for field measurement of leaf transmittance", Optical Engineering, **26** (12), 1191-1196 (1987)

8. A.F.H. Goetz, G. Vane, J. Solomon, B.N. rock, Science **228**, 1147 (1985)

9. J.R. Schott, "Remote Sensing of the Earth: A Synoptic View", Physics Today, (1989)

10. Warren J. Smith, Modern Optical Engineering, McGraw Hill (1966)

11. John A. Duffie, William A. Beckman, Solar Energy Thermal Processes, John Wiley and Sons (1979)

12. A. Girard and P. Jacquinot, "Principles of Instrumental Methods in Spectroscopy", from Advanced Optical Techniques edited by A.C.S. Van Heel, North-Holland Publishing Co.

13. Robert W. Boyd Radiometry and the Detection of Optical Radiation, John Wiley and Sons (1983)

14. The Photonics Buyers' Guide to Products and Manufacturers, from the Publishers of Photonics Spectra Magazine

15. Xiaofan Feng, "Comparison of Methods for Generation of Absolute Reflectance Factor Measurements for BRDF Studies" Center for Imaging Science Thesis, RIT (1990)

16. Walter G. Egan, "Polarization in Remote Sensing", Proc. SPIE **891** 2 - 9 (1988)

17. Kinsell L. Coulson, "Polarization of Light in the Natural Environment", Proc. SPIE **1166** 2 - 10 (1989)

APPENDIX A

Pixel Summing

A.1 CCD Imager Archetecture

The imager used for this project is a Toshiba TCD105C linear image sensor. This imager has 3648 8μm x 8μm image sensing elements on 8μm centers. The incident light is photoelectrically converted to a current by pn photodiodes, and this current then becomes the signal charge stored in the MOS capacitor. The signal charge is then shifted to the transfer region by means of the shift gate (see figure A-1). The transfer region consists of a dual channel CCD analog shift register, one shift register accommodates charges from even numbered photosites and the other is for charges from the odd numbered photosites. These shift registers transport the individual charge packets to the output circuit region (output stage) where each bucket of signal charge is converted into a voltage signal and is then stored in a floating capacitor with a reset function. The output stage must hold the voltage level long enough to be amplified, if required, and digitized. Once the digitization process is completed, the *reset clock* is exerted, which activates the reset gate and resets the output stage to ground state, then pixel clock transports the next charge into the output stage for processing. Imperfections in either the imager or the control electronics can cause the output stage to incompletely reset to a level which is not at ground, and this *residue level* may vary from pixel to pixel. This pixel to pixel variation can be eliminated by *correlated double sampling* (CDS), which consists of digitizing the residue level and the signal level, the difference between these two levels being the actual charge transferred from the shift register to the output stage. CDS effectively eliminates KTC noise in the capacitor and any low frequency (eg. 60 Hz.) noise infiltrating the output signal.

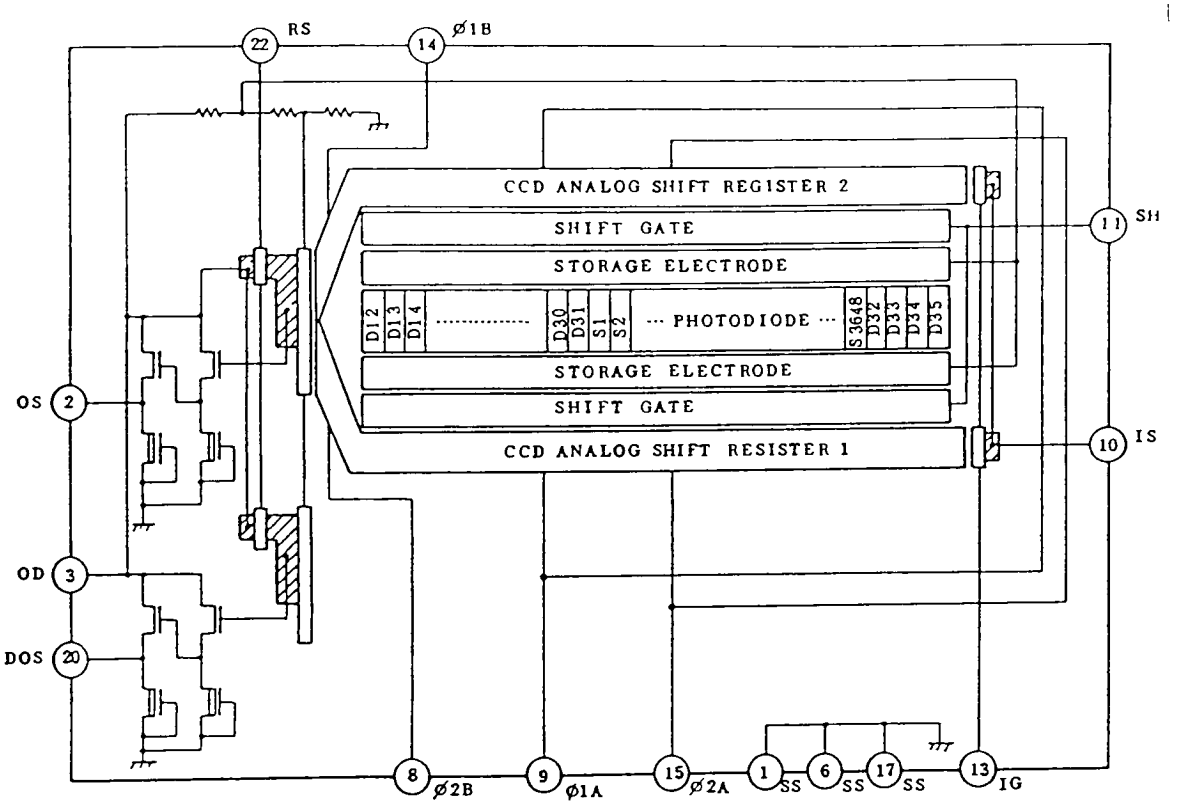

Figure A-1 CCD Imager Archectecture

The timing clocks necessary to operate the imager are pictorially represented in figure A-2. The first clock is termed *new line* because it determines the amount of time the photosensitive elements have to accumulate photons (*integration time*) for one line of imager data. When new line is exerted, each individual bucket of charge which has been accumulated by the photosensitive elements is transferred into the appropriate CCD shift register. Once these charges are transferred to the CCD shift registers, *pixel clock* is used to transport the charges, in increments of one CCD shift register, to the output stage, which is the final destination on the imager for these individual buckets of charge.

Pixel clock actually consists of two separate clocks which are identical except for a 180^{0} phase shift. Under normal operating conditions the floating capacitor in the output stage is reset just prior to the next charge being shifted in.

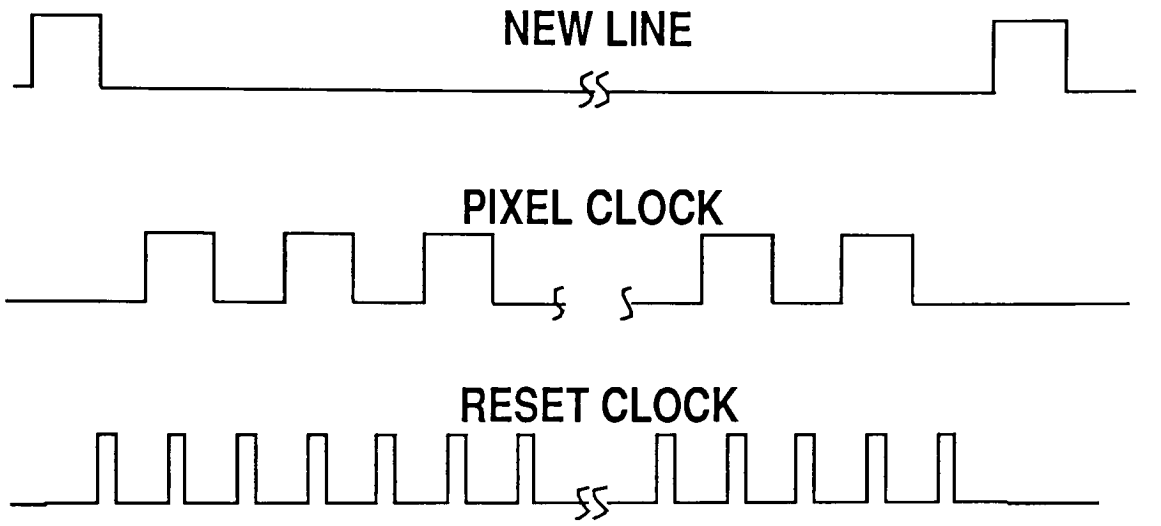

Figure A-2 CCD Imager Clocks

A.2 Noise Analysis

The noise encountered when using charge coupled device (CCD) imagers can be separated into two classes. The first noise class, denoted here as n_{det}, occurs during the conversion of photons to electrons and collection of the electrons by the photosite. Such noise sources include quantum noise of photon detection (signal-dependent Poisson noise) and the detector physics (thermally generated dark current noise).

$$(n_{phot})^2 = E + d^2$$

E = s·t, signal level per photosite

d = d (t,T), dark noise

s = rate at which electrons are produced

t = time in seconds

T = temperature (K)

This detector noise is present in every photosite, and, under stable operating conditions, will sum in quadrature with the number of photosites, independent of sampling scheme.

The second noise class includes systematic variations and analog circuitry noise associated with transporting and sampling the analog signal. Such noise sources include internal CCD clock noise, kTC noise in the output stage reset level, inductive coupling of radiated signals, thermal (Johnson) noise in resistors and noise from active analog devices. All of these sources combine to form one large, signal-independent variance with a Gaussian distribution.

$$(n_{sys})^2 = (n_{clk})^2 + (n_{kTC})^2 + (n_{thermal})^2$$

This systematic noise, which can be minimized with more extensive analog circuit design and correlated double sampling (CDS),will sum in quadrature with each CDS sampling pair.

Digitally summing m pixels requires m CDS pairs per pixel, and the resulting variance is:

$$(n_{digital})^2 = m\cdot[(n_{sys})^2 + (n_{det})^2]$$

The signal increases by a factor of m, and the RMS noise increases by a factor of square root of m. Digital summing increases the signal to noise ratio by root m.

Analog summing of m adjacent pixels requires only one CDS pair, and the resulting variance in this case is:

$$(n_{analog})^2 = (n_{sys})^2 + m \cdot (n_{det})^2$$

Analog summing on the output capacitor can only occur at low signal levels, where the signal dependent noise term (photon Poisson noise) is small. Assuming the CCD array is reasonably stable (low dark noise), systematic noise is truely dominant at these signal levels, and it is independent of the number or photosites summed (m)! Analog summing increases the signal to noise ratio by a factor of m.

The front end electronics used on this project is capable of performing an adaptive, real time *pixel* summing scheme that utilizes analog *or* digital pixel summing, based upon signal level to optimally increase the dynamic range of the system. The digitized CCD data is presented to a hardware processing unit that acts as both an interface to the data storage device and controller of clocks on the CCD array. If the *first-of-4* data level is below a predetermined threshold, the CCD array clocks are modified to allow the next 3 charges to accumulate in the output stage of the CCD array (*analog* summing). If the first-of-4 data level is above the predetermined threshold, the processing unit switches to *digital* summing and the next 3 pixel values are digitally added to the first-of-4 value.

A.2 Pixel Summing

The output signal one would see when monitoring the output stage is represented in figure A-4. Under normal operating conditions this signal consists of a narrow, negative voltage reset feed-through pulse, followed by the residue level, then the signal level. The positioning of the reset pulse relative to the pixel clock determines the temporal width of the residue and data levels. The output stage is capable of holding at least as much charge as is contained

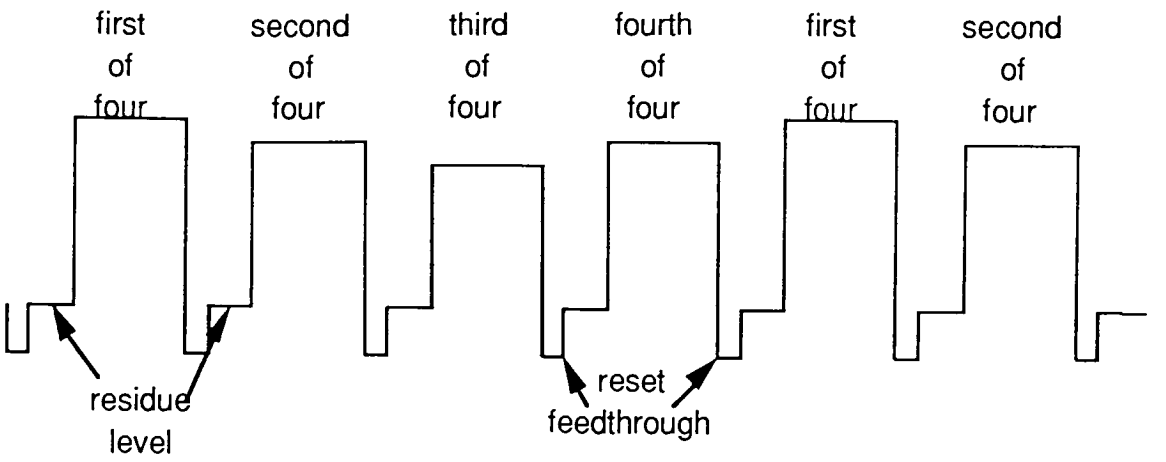

Figure A-4 Normal CCD Output

in one photosite which has been illuminated to full well; therefore, the output stage could hold the total charge contained in several dimly illuminated photosites. Figure A-5 illustrates the accumulation of charge in the output stage that would occur if the reset pulse for three out of every four dim pixels were inhibited. The difference between signal level four and the residue level represents the total accumulated charge from the previous four photosites. The figure shows output stage pixel summing of four adjacent pixels; however, any number (m) of photosite charges may be accumulated, provided the total charge level does not exceed the total range of the output stage.

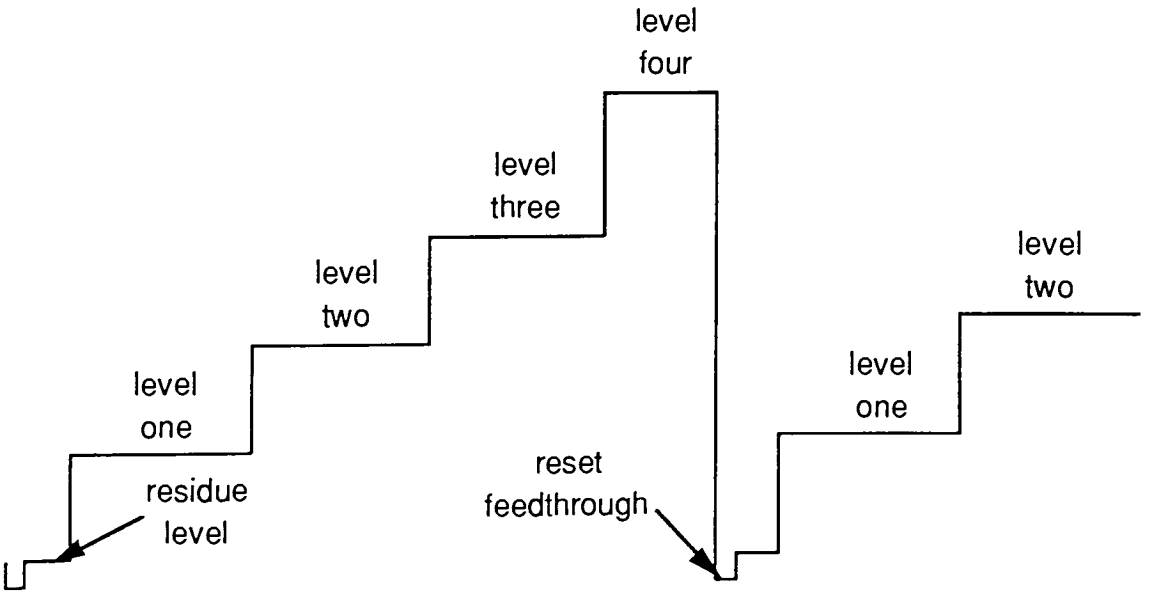

Figure A-5 CCD Output With Analog Summing

Figures A-6 and A-7 are actual scope traces of CCD output under normal operation and analog summing respectively.

T/div .2 µs Ch 2 50 mV =

Figure A-6 Normal Operation CCD Output

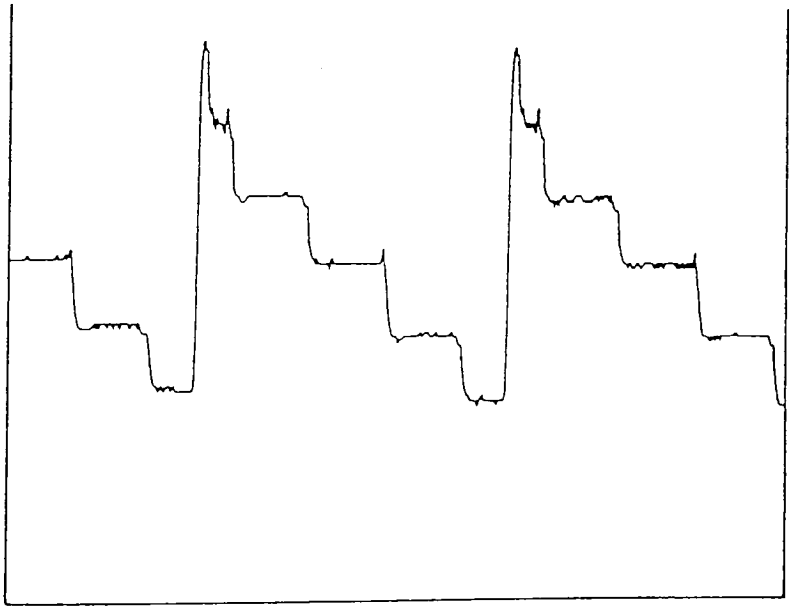

T/div .5 µs Ch 2 50 mV =

Figure A-7 CCD Output With Analog Summing

Figure A-8 is a block diagram of the scanning system that utilizes the analog / digital pixel summing technique (and line summing if desired). The essential componenents of the system are:

* **linear CCD sensor** and the analog electronics required to operate it

* **analog to digital converter** with sample and hold and other required analog and digital electronics

* **arithmetic logic unit (ALU)** with digital electronics necessary to operate the ALU and generate the CCD imager clocks and the A/D strobe

* **computer I/O card** to allow data storage

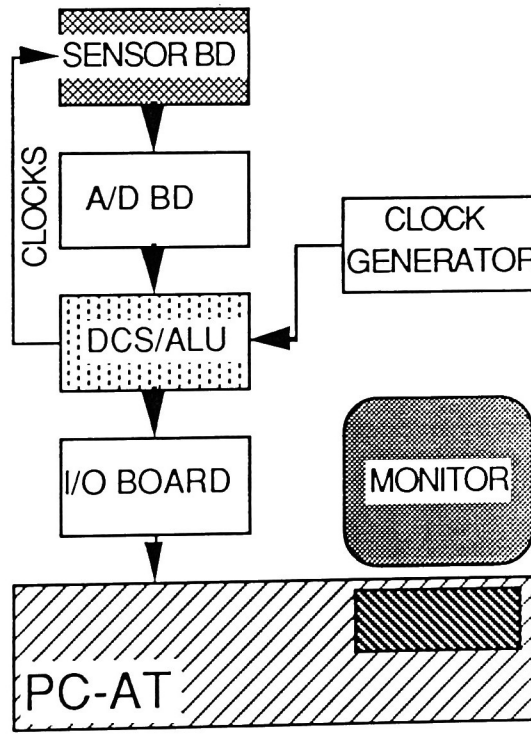

Figure A-8 Electronics Block Diagram

The ALU board is the central component in the pixel summing scanner. Figure A-9 is a flow chart of the decision making process for analog verses digital summing. Following this flow chart, and referring to the imager output signals shown in figures A-4 and A-5, note that the first piece of information presented to the ALU board from the A/D board is the residue level preceding the first of the four photosite charges to be summed, and this value is stored. Next, the ALU board receives the digitized first-of-four charge level and subtracts the stored residue level from it. If the resultant is less than a predetermed threshold level, which is about one eighth the full well value for one photosite, then the ALU board inhibits the next three reset pulses, waits for level four data level, subtracts the stored residue level from the level four data level and sends the resultant to the input master along with a data ready pulse. If the resultant of data level one minus residue is greater than the predetermined threshold, then the ALU board retains this resultant, enables the next three imager reset pulses, and successively subtracts the residue level and adds the data level for the next three photosite charges. The resultant of these four digitally summed photosites is then sent to the computer I/O card along with a data ready pulse. Once this four photosite sequence is completed, the ALU is reset and ready for the next four photosites. The imager new line clock will cause the ALU board to exercise the beginning of line sequence, where the ALU waits for the predetermined first imager photosite to begin pixel summing.

In conclusion, the pixel summing technique uses more than one photosite per pixel to improve the quantized data signal-to-noise ratio. This technique requires a prion knowledge of the image to be scanned in that there are no high frequency density fluctuations. That is to say, we assume that, given the first-of-four photosite charge content is one eighth the capacity of the output stage, the image will not vary fast enough to overflow the output stage after accumulating the next three photosite charges. This is a valid assumption as the input slit is the limiting factor in system resolution, effectively filtering high frequency fluctuations .

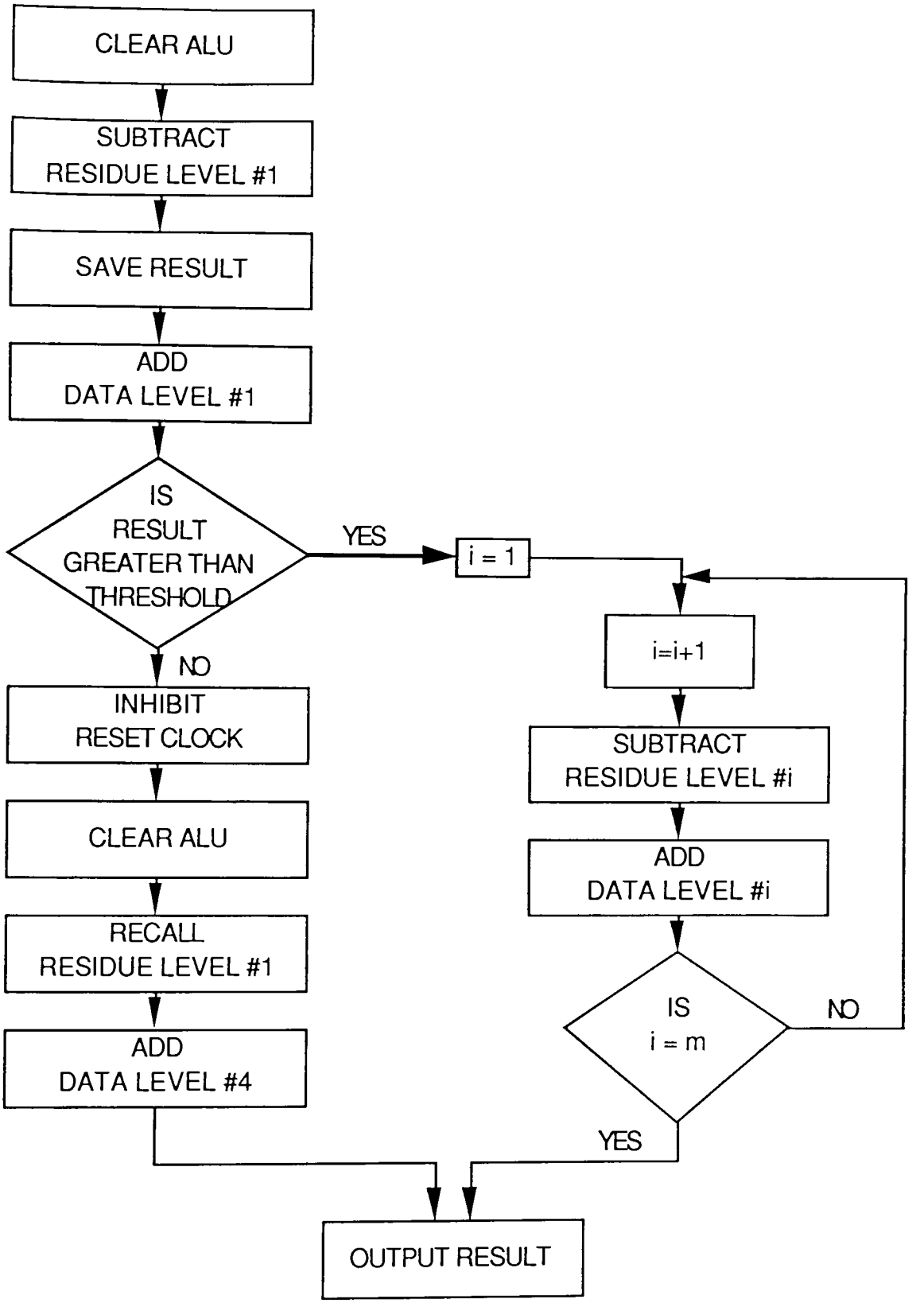

Figure A-9 Pixel Summing Electronics Flow Chart

APPENDIX B - INCIDENT SOLAR ANGLE

The gain corrections are acquired by viewing a flat piece of Spectralon which is lying flat on the ground at the zenith angle (0 degrees declination). The reflectance of the Spectralon varies with the angle of incidence of the illumination (Feng), so we must know this incident angle when corrections are performed. The geometric relationships between a plane of any particular orientation relative to any point on the earth at any time and the position of the sun relative to that plane can be described in terms of several angles (Duffee, 1979). These angles, and the relationships between them are:

ϕ = latitude (north positive)
δ = declination, angular position of the sun at solar noon w/r to the equator
s = angle between the object and horizontal (slope of object w/r to flat ground)
γ = object surface azimuth angle
ω = hour angle, solar noon = 0, morning positive, afternoon negative
θ = angle of incidence of beam radiation, measured from zenith

Since the Spectralon sample is lying flat on the ground, s and γ are both zero.

The declination from zenith, δ , (in degrees) can be found from the approximate equation of Cooper (1969) :

$$\delta = 23.45 \sin[(284 + n)(360/365)]$$

where n is the day of the year. The relationship between θ and the other angles, with s and γ both 0, is given by:

$$\cos \theta = \sin \delta \sin \phi + \cos \delta \cos \phi \cos \omega$$

The solar time rarely coincides with the local time, and must be computed. The way that I have chosen is to compute Greenwich Mean Time (GMT) and adjust to local solar time by realizing that every 15 degrees longitude is equal to a 1 hour time difference. A second correction is from the equation of time which takes into account the various perturbations in the earth's orbit and rate of rotation which affect the time the sun appears to cross the observers meridian. Figure B-1 shows a plot of this variation (in minutes) against the year day.

In order to account for the emperical perturbation data, a cosine series approximation to the data was determined and is also plotted in figure B-1. The general form of the cosine series is:

$$f(t) = a_0 + \sum_{i=0}^{n} a_i \cos((2\, i\, \pi / L) + b_i)$$

t = time (days) L = period (365 days)

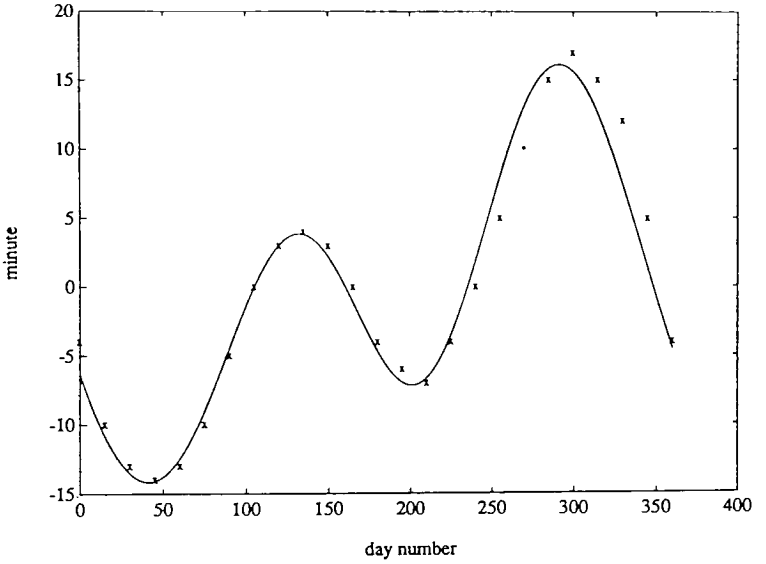

i	a_i	b_i
0	0.400	
1	7.974	1.699
2	9.540	2.171
3	1.244	-1.201

Figure B-1 Solar Noon Pertabations vs Year Day and third order cosine series

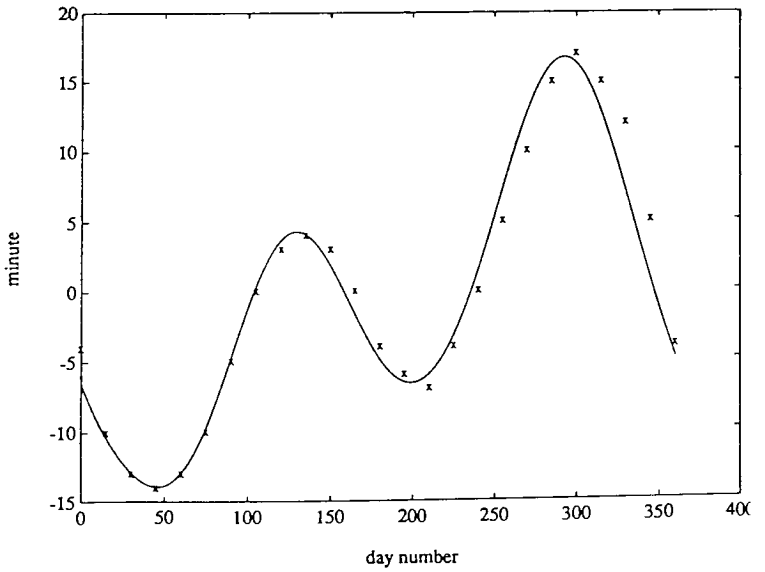

i	a_i	b_i
0	0.400	
1	7.974	1.699
2	9.540	2.171
3	1.244	-1.201
4	0.6737	-1.793

Figure B-2 Solar Noon Pertabations vs Year Day and fourth order cosine series

APPENDIX C
BUSTER FIELD SETUP

1) Roughly level triopod using 3 built in buble levels.

2) using compass, point monochromator due south and record rotation angle.

3) Level Oriel monochromator front to back by adjusting front tripod leg.

4) Level Oriel monochromator left to right and record declination angle.

5) Using plumb line, locate 0° spot and record lens to ground distance.

6) Place spectralon at 0° location and level spectralon. (use loop brdf plot to make sure spectralon is positioned correctly and check signal level)

7) Make sure digital electronics is functional with count up diagnostics.

8) Check CCD sensor DC offset level, should be between 150 and 300 counts.

9) Check defaults to assure setup is as required for the job.
lambda inc - angle inc - declination angle lattitude longitude - deg true N
move mtrs (yes) - apply crct (yes) - use diode (yes)

10) Implement *point true south* command.

11) Cover reference photodiode and lens and acquire dark corrections.

12) Uncover reference photodiode and lens and acquire gain corrections.

13) Remove spectralon and perform BRDF run.

EQUIPMENT NEEDED

compass - small level - plumb line - tape measure

NOTES

Repeat steps 10 - 11 for each BRDF, fresh dark and gain values are critical. 0° rotation and declination readings should be verified before each BRDF run. Reference photodiode must be pointed at a diffuse white reflector and remain stationary during the data collection cycle.

The signal level can be adjusted by:

1) changing the base frequency crystal oscillator on the clock board
2) adjust the gain pot on the imager board, which affects theDC offset level so you must adjust the offset pot also.